TRPV4 overactivation enhances cellular contractility and drives ocular hypertension in TGFβ2 overexpressing eyes

Christopher N. Rudzitis[1,2], Monika Lakk[1], Ayushi Singh[3,4], Sarah N. Redmon[1], Denisa Kirdajova[1], Yun-Ting Tseng[1], Michael L. De Ieso[5], W. Daniel Stamer[5], Samuel Herberg[3,4,6] and David Križaj[1,2,7]

[1]Department of Ophthalmology and Visual Sciences; and [2]Department of Neurobiology, University of Utah, Salt Lake City, UT; [3]Department of Ophthalmology and Visual Sciences; [4]Department of Cell and Developmental Biology, SUNY Upstate Medical University, Syracuse, NY; [5]Department of Ophthalmology, Duke Eye Center, Duke University, Durham, NC;[6]Department of Biochemistry and Molecular Biology, SUNY Upstate Medical University, Syracuse, NY; [7]Department of Bioengineering, University of Utah, Salt Lake City, UT

**** Corresponding author.*** David Križaj, 65 N Mario Capecchi Drive, Bldg. 523, Room S4140 JMEC, Salt Lake City, UT 84132. david.krizaj@hsc.utah.edu

COI: The authors declare no conflict of interest, financial or otherwise. D.K. is a cofounder of TMClear and co-inventor of patents (US 2015/0133411, US20230026696) related to the development of cornea-permeant TRPV4 channel antagonists. The patents were licensed to TMClear by the University of Utah.

Abstract

The risk for developing primary open-angle glaucoma (POAG) correlates with the magnitude of ocular hypertension (OHT) and the concentration of transforming growth factor-β2 (TGFβ2) in the aqueous humor. Effective treatment of POAG requires detailed understanding of interaction between pressure sensing mechanisms in the trabecular meshwork (TM) and biochemical risk factors. Here, we employed molecular, optical, electrophysiological and tonometric strategies to establish the role of TGFβ2 in transcription and functional expression of mechanosensitive channel isoforms alongside studies of TM contractility in biomimetic hydrogels, and intraocular pressure (IOP) regulation in a mouse model of TGFβ2 -induced OHT. TGFβ2 upregulated expression of *TRPV4* and *PIEZO1* transcripts and time-dependently augmented functional TRPV4 activation. TRPV4 activation induced TM contractility whereas pharmacological inhibition suppressed TGFβ2-induced hypercontractility and abrogated OHT in eyes overexpressing TGFβ2. *Trpv4*-deficient mice resisted TGFβ2-driven increases in IOP. Nocturnal OHT was not additive to TGFβ-evoked OHT. Our study establishes the fundamental role of TGFβ as a modulator of mechanosensing in nonexcitable cells, identifies TRPV4 channel as the final common mechanism for TM contractility and circadian and pathological OHT and offers insights future treatments that can lower IOP in the sizeable cohort of hypertensive glaucoma patients that resist current treatments.

Introduction

Primary open-angle glaucoma (POAG) is an irreversible blinding disease afflicting ~3.5% of the global population (1). Its incidence and severity are proportional to the amplitude and duration of ocular hypertension (OHT) (2, 3), which correlates with retinal ganglion cell dysfunction, neuroinflammation, and oxidative stress (4, 5). Biomechanical factors, glucocorticoids, and the cytokine transforming growth factor-β2 (TGFβ2) contribute to POAG by compromising the funneling of aqueous humor (AH) from the trabecular meshwork (TM) into the canal of Schlemm (SC). IOP elevations increase the contractility of juxtacanalicular TM (JCT), a circumocular tissue formed by extracellular matrix (ECM) beams populated by mechanosensitive cells smooth muscle-like cells, by increasing its resistance to the flow of aqueous humor (AH). The molecular mechanism that links TM pressure sensing to the contractile response is not known but is likely to underpin the uts sensitivity to compressive, tensile, osmotic, shear and traction forces to regulate the expression of hundreds TM genes and secretion of dozens of ECM proteins (6–12).

The increase in trabecular outflow resistance induced by mechanical stress, glucocorticoids, and TGFβ2 consists of a dynamic component that can be reversed by cytoskeletal and Rho signaling blockers, and a chronic component, reflecting transdifferentiation of TM cells into fibrotic and contractile myofibroblasts (16–18). One of the clearest examples of fibrotic remodeling in glaucoma pertains to TGFβ2 signaling: (i) TM cells derived from POAG patients secrete more active TGFβ2 compared to cells isolated from healthy donors (19), (ii) the likelihood of contracting POAG is proportional to $[TGF\beta2]_{AH}$ (20–22), and (iii) ocular overexpression of TGFβ2 is sufficient to induce OHT (23, 24), presumably due to overexpression of ECM proteins and increased cellular contractility (25, 26). The cognate TGFβ1 isoform similarly induces fibrotic remodeling in fibroblasts, epithelial, and endothelial cells in the heart, kidney, skin, and lung (27–30). TGFβ overexpression is thus a causal determinant of OHT that may reflect a universal fibrotic program that, however, cannot be disambiguated from the biomechanical environment. TGFβ release is activated by tissue contractility and tension (31, 32), TGFβ activity

63 correlates with the distribution of mechanical stress (33), and mechanical stress may induce TGFβ -
64 dependent epithelial-mesenchymal transition (EMT; 34, 35).

65 Our understanding of TM mechanotransduction and its role in IOP homeostasis remains
66 rudimentary despite its overarching clinical relevance. Strain and shear were proposed to stimulate the
67 TM primary cilium, integrins and TRPV4, Piezo1 and TREK-1 channels (36–39) but it is not clear
68 whether mechanosensation regulates TM contractility or is itself impacted by POAG inducers (e.g.,
69 TGFβ2 or glucocorticoids) nor is it known how it relates to chronic fibrosis. TRPV4 (Transient Receptor
70 Potential Vanilloid isoform 4), a tetrameric channel with P_{Ca}/P_{Na} ~ 10 (40), is strongly expressed in rodent
71 and human TM (36, 51) where it carries the principal component of the pressure-activated transmembrane
72 current and stretch-evoked $[Ca^{2+}]_i$ elevations together with responsiveness to shear and swelling (7, 10,
73 37, 39, 41, 42). Pharmacological inhibition of the channel and deletion of the TRPV4 gene modulate
74 pressure gradients in the brain, kidney, lung, and bladder (46–50) and mutations in the TRPV4 sequence
75 underpin sensorimotor neuropathies, skeletal dysplasias, retinal degeneration and ocular dysfunction (43–
76 45) while the function of TRPV4 channels in ocular hypertension remains under debate. TRPV4 activity
77 has been implicated in IOP lowering and elevation, respectively and linked to a diverse array of effector
78 mechanisms that include eNOS and RhoA activation, phospholipid-cholesterol-caveolin regulation,
79 modulation of cell-ECM contacts, primary cilia mechanosensing, polyunsaturated fatty acid release, and
80 Piezo1 signaling (7, 37, 41, 52–55). This invites testable predictions regarding TRPV4 involvement in
81 ocular function and POAG. If TRPV4 maintains steady-state normotension, opposes the profibrotic
82 effects of TGFb2 and promotes outflow via eNOS-dependent TM relaxation (7, 52), abrogation of its
83 activation should elevate IOP. Conversely, if TRPV4 promotes OHT (37), its inhibition of deletion of the
84 TRPV4 gene should lower IOP.

85 In this study, we demonstrated novel functions for the TRPV4 channel in homeostatic and
86 pathological IOP regulation by uncovering the mechanisms through which reciprocal TRPV4-TGFb2
87 interactions maintain the vicious cycle between mechanical stressors and TM contractility that underlies

OHT. We found that inhibition and deletion of TRPV4 lower IOP in TGFβ2 overexpression-induced and circadian models of OHT and suppress TM contractility in TGFβ2-treated biomimetic hydrogels. The cytokine promoted upregulation of EMT-associated genes alongside increased transcription and trafficking of TRPV4, which may have increased the sensitivity of TM cells to innocuous mechanical stimuli. While physiological (nocturnal) and pathological (cytokine-induced) OHT modes both required TRPV4 activity they were not additive, indicating the involvement of a final common pathway. Collectively, we identify TRPV4 as a fulcrum of TGFβ2 -induced TM contractility and IOP regulation and a candidate target for glaucoma therapy.

Results

TGFβ2 drives overexpression of genes that encode fibrotic markers and mechanosensitive ion channels

Human TM cells respond to TGFβ2 with increased biosynthesis, deposition and degradation of ECM, altered autophagy, upregulation of F-actin stress fibers, a-smooth muscle actin (aSMA) (19, 25, 26, 56, 57), but it is unclear whether cells undergoing TGFβ2-induced fibrotic remodeling also exhibit altered capacity for sensing and transduction of mechanical stimuli. We profiled genes that encode known TM mechanochannels together with a selection of key cytoskeletal, ECM, and fibrotic markers in primary TM cells (pTM) isolated from 3-7 donors without history of visual dysfunction (Figure 1*A*-*C*). Five-day exposure of pTM cells to a physiological concentration of TGFβ2 (1 ng/mL) increased the expression of EMT-promoting transcription factor SNAI1 (*SNAIL1*, $P = 0.0094$) and fibronectin (*FN1*, $P = 0.0263$), while expression of connective tissue growth factor *2* (*CCN2*, alternatively *CTGF*) was elevated in 5/5 pTM cell strains without reaching significance ($P = 0.0909$). Expression of fibroblast-specific protein 1 (*FSP1*, a calcium-binding fibroblast marker), yes-associated protein 1 (*YAP1*, a stiffness induced hippo-pathway transcription factor) and *ACTA2* (αSMA, associated with cell contractility) was not consistently impacted by TGFβ2 while transcription of myocilin (*MYOC*) decreased across 4/4 pTM strains ($P = 0.0055$) (Figure 1*B*). Indicative of feedback inhibition (58), TGFβ2-treatment downregulated transcript

levels of transforming growth factor beta receptor 2 (*TGFBR2*, $P = 0.0219$) and upregulated expression of autoinhibitory SMAD family protein 7 (*SMAD7*, $P = 0.0461$) without affecting *SMAD2* or *SMAD3* expression. TGFβ2 thus promotes selective upregulation of ECM and fibrosis-related genes together with cell dedifferentiation and activation of autoregulatory SMAD mechanisms.

Analysis of genes encoding mechanosensitive channels implicated in outflow modulation (36, 39, 59, 60) showed a 102.5% increase in expression of *TRPV4* ($P = 0.0193$) and 78.9% increase in *PIEZO1* expression ($P = 0.0114$) across 8 replicates including 7 distinct pTM strains. (Figure 1*C*). Conversely, TGFβ2 exposure did not affect *TRPC1* gene expression ($P = 0.261$) and had variable, strain-dependent effects on transcript levels *of KCNK2 (*$P = 0.293$, encoding the TREK-1 channel). Thus, TGFβ2 promotes selective transcriptional upregulation of genes that encode a subset of mechanosensitive proteins alongside fibrotic upregulation and cell dedifferentiation.

TGFβ2 exposure time-dependently augments TRPV4-mediated current and $\Delta[Ca^{2+}]_i$

To assess the functional relevance of TGFβ2-dependent transcriptional upregulation we determined the membrane expression and functional activation of TRPV4, which mediates the pressure-activated current and calcium signaling, regulates cytoskeletal dynamics and modulates conventional outflow resistance in vitro (37, 41). Western blots showed that TGFβ2 exposure produces an increase in levels of membrane-bound TRPV4 protein (Figure 1*D*) in two grouped pTM membrane protein samples. While low amounts of TRPV4 were visible in the membrane fractions in control samples, TGFβ2 treatment produced an increase in the higher weight TRPV4 band, suggesting there could be isoform-specific TGFβ2-induced responses and increased TRPV4 translation leading to elevated TRPV4 trafficking, membrane insertion and/or lipid raft interaction (52).

Functional expression was assessed by tracking $[Ca^{2+}]_i$ changes in cells exposed to the selective TRPV4 agonist GSK1016790A (GSK101, 10 nM) using Fura2-AM ratiometric Ca^{2+} dye, with TGFβ2-treated and control cells tested on the same day. All pTM strains responded to GSK101 with robust $[Ca^{2+}]_i$

increases which reached peak within 5 min before the majority of responding cells gradually decreased to a steady plateau (Figure 2*C*). TGFβ2-treated cells exhibited a remarkable potentiation of GSK101-evoked $[Ca^{2+}]_i$ responses compared to control cells, with 5/5 cell strains showing an increase in the Δpeak/baseline F_{340}/F_{380} response equivalent to 258.4% ± 61.7% of the control response in ($P = 0.0046$) (Figure 2*A*-*B*). The fraction of GSK101 responders and the overall time course of responses between groups were not significantly different, indicating that TRPV4 potentiation primarily affects TRPV4-expressing cells. Thus, TGFβ2 treatment promotes TRPV4 expression and functional activity.

To gain insight into the time- and dose-dependence of TGFβ2-dependent TRPV4 signaling modulation pTM cells were treated for 24 hours, at 1 ng/mL and 5 ng/mL concentrations of TGFβ2. GSK101-stimulated Ca^{2+} influx was not significantly increased by 24-hour TGFβ2 treatment at 1 ng/mL (Δpeak/baseline F^{340}/F^{380} = 117.0% ± 23.6% of control) or 5 ng/mL (Δpeak/baseline F^{340}/F^{380} = 133.6% ± 34.5% of control) (Figure 3; SI Appendix, Figure S1); additionally, the potentiation of both was significantly lower relative to the five-day 1 ng/mL TGFβ2 treatment ($P < 0.0011$; Figure 3*A*). GSK101 evoked a moderately outwardly rectifying nonselective current (I_{GSK}-$I_{baseline}$) with reversal potential at ~0 mV (Fig 3*C*). While its amplitude was variable, mean current density consistently increased in cells treated for 1 day with TGFβ2 (n = 10; 5 ng/mL) relative to the control group (n = 11). The potentiating effect of TGFβ2 on TRPV4 activity thus appears to be time-dependent but is significant after chronic exposure to relatively low-dose TGFβ2.

TGFB2-Induced TM contractility requires TRPV4 activation

The IOP-lowering effectiveness of Rho kinase inhibitors and latrunculins (57, 61–63) indicates that sustained increases in outflow resistance require tonic actin polymerization and contractility. TGFβ2 drives the TM myofibroblast contractile response (57) while the role of mechanosensation remains unknown. To ascertain whether TRPV4 upregulation (Figures 1-2) contributes to the contractile response, we seeded pTM cells into high-compliance Type I collagen hydrogels (57) (Figure 4, SI Appendix, Figure

S2). Hydrogels that were incubated with TGFβ2 (5 ng/mL) showed profound increases ($P < 0.0003$) in the rate and the magnitude of contraction at all time points (Figure 4, SI Appendix Figure S2). Simultaneously, treatment with the TRPV4 antagonist HC-067047 (HC-06, 5 µM) significantly reduced the extent of TGFβ2-induced TM contractility ($P < 0.0001$). To determine whether TRPV4 activation is sufficient to induce the contractile response, the antagonist was washed out and hydrogels supplemented with GSK101 (25 nM). 15 minutes post-treatment, the constructs responded to the agonist with transient contraction (Figure 4*C*; SI Appendix, Figure S2, $P < 0.01$), with a time course mirroring GSK101-induced $[Ca^{2+}]_i$ elevations (Figures 2-3). The effects of TRPV4 inhibition and activation were consistent across all pTM strains tested (N = 3 pTM strains). TRPV4-mediated $Ca2^{2+}$ influx is therefore sufficient to induce TM contractility and necessary for pTM hypercontractility induced by TGFβ2.

TRPV4 activation is required to maintain TGFβ2-induced OHT

To test whether TRPV4 contributes to TGFβ2 induced ocular hypertension (OHT) *in vivo*, we utilized the lentiviral TGFβ2 overexpression model developed by Patil et al. (23). Adult C57BL/6J mice (N = 5) were intravitreally injected with lentivirus overexpressing constitutively active human TGFβ2 (LV-TGFβ2). LV-TGFβ2-injected eyes, but not the contralateral eyes injected with a lentivirus containing a scrambled transgene (LV-Ctrl), exhibited significant IOP elevations one-week post-transduction (Figure 5*A*, Week 2, $\Delta_{TGF\text{-}Ctrl} = 4.0$ mm Hg, $P = 0.0143$). By 2 weeks post-transfection, IOP in LV-TGFβ2 eyes reached 19.9 ± 4.7 mm Hg whereas IOP in LV-Control eyes remained at control levels (14.0 ± 1.2 mm Hg), with $\Delta_{TGF\text{-}Ctrl} = 5.9$ mm Hg ($P = 0.0002$). IOP remained elevated throughout the 4 weeks after the injection (Week 5, $\Delta_{TGF\text{-}Ctrl} = 4.9$ mm Hg, $P = 0.0008$). HC-06 (100 µM) microinjection into the anterior chamber of LV-TGFβ2 and LV-Ctrl eyes lowered IOP in LV-TGFβ2 eyes to 12.2 ± 1.7 mm Hg after 24 hours ($\Delta_{postHC\text{-}preHC} = -5.8$ mm Hg) with no difference observed in IOP from LV-Ctrl eyes (12.6 ± 1.9 mm Hg, $\Delta_{post\text{-}HC\text{-}pre\text{-}HC} = -0.3$ mm Hg). LV-Ctrl eyes remained close to pre-injection levels post-HC-06 treatment (Figure 5*A*-*B*). IOP in LV-TGFβ2 eyes returned to hypertensive levels by 1-week post-HC-06 injection (Week 6-7, $\Delta_{TGF\text{-}Ctrl} = 3.9$ mm Hg, $P = 0.0201$). To determine the effect of the bolus injection

alone, LV-TGFβ2 and LV-Ctrl eyes were reinjected with PBS 2 weeks after re-establishing the OHT baseline. The sham injection transiently reduced IOP in LV-TGFβ2 ($\Delta_{postPBS\text{-}prePBS}$= -4.5 mm Hg) and LV-Ctrl ($\Delta_{postPBSpre\text{-}PBS}$= -1.2 mm Hg) eyes; however, LV-TGFβ2 eyes returned to hypertensive levels by 48 hours post-injection ($\Delta_{TGF\text{-}Ctrl}$ =3.6 mm Hg, p=0.0465) and to pre-injection levels after 72 hours ($\Delta_{TGF\text{-}Ctrl}$ =5.4 mm Hg, p=0.0002). Bolus injection was less effective than HC-06 at all time points 24 hours post-injection (Week 8-9, Figure 5*B*). These data indicate that selective pharmacological inhibition of TRPV4 effectively and reversibly blocks TGFβ2-induced OHT.

To further evaluate the TRPV4-dependence of TGFβ-induced OHT we took advantage of mice with global *Trpv4* knockdown (64–66). *Trpv4*$^{-/-}$ mice (N = 6) were injected with LV-TGFβ2 and LV-Ctrl vectors in contralateral eyes (Figure 5*C*). Additionally, two littermate control mice injected alongside the *Trpv4*$^{-/-}$ animals were added to previously collected WT LV-injected cohorts measured at the same timepoints (N = 8-15, Figure 5*C*). Pre-LV injection, IOP levels in *Trpv4*$^{-/-}$ animals were comparable to the WT cohort, indicating that TRPV4 activity does not regulate normotension. Similarly, IOP in LV-Ctrl-injected eyes was not significantly different between WT and *Trpv4*$^{-/-}$ animals at any point in the experiment (peak $\Delta_{CtrlKO\text{-}CtrlWT}$ = -1.2 mm Hg, SI Appendix, Figure 5*D*). By two weeks post-injection (Week 3), LV-TGFβ2-treated *Trpv4*$^{-/-}$ eyes exhibited significantly lower IOP compared to the LV-TGFβ2 WT cohort ($\Delta_{TGFKO\text{-}TGFWT}$ = -3.1 mm Hg, *P* =0.0009, Figure 5*C*). While LV-TGFβ2 injected *Trpv4*$^{-/-}$ eyes exhibited mild OHT, the effect was significantly reduced compared to WT eyes and IOP decreased by two weeks post-injection (Figure 5*C-D*).

TGFβ2-induced and nocturnal OHT are non-additive but require TRPV4

Mammalian IOP is modulated by the circadian rhythm, with levels elevated at night and nocturnal IOP fluctuations implicated in POAG (7, 55, 67). We measured nocturnal (9:00-10:00 PM) IOP in LV-TGFβ2 and LV-Ctrl WT eyes (N=4) to determine whether nocturnal OHT is additive to elevation observed during the daytime (12:00-2:00 PM, Figure 6*A*). LV-TGFβ2 injected eyes showed significant IOP elevation compared to LV-Ctrl eyes during daytime measurements (Diurnal $\Delta_{TGF\beta\text{-}Ctrl}$ = 7.9 mm Hg, *P*

211 < 0.0001) but the difference vanished at night (Nocturnal $\Delta_{TGF\beta\text{-}Ctrl}$ = 0.2 mm Hg), indicating that TGFβ2-
212 induced OHT is not additive to the circadian OHT. To determine whether physiological (nocturnal) OHT
213 requires TRPV4 we microinjected the eyes of two animals with PBS, and two with HC-06. When IOP
214 stably recovered after the first treatment, the treatment groups were switched. PBS injection did not affect
215 IOP in LV-Ctrl or LV-TGFβ2 eyes at day or night (Figure 6*B*-*C*) except for a single LV-TGFβ2 eye
216 exhibiting abnormally high nocturnal IOP (37 mm Hg) at the four-day timepoint. Conversely, HC-06
217 injection blocked LV-TGFβ2-induced IOP during the day ($P < 0.001$) and significantly lowered IOP ~5
218 mm Hg in both LV-Ctrl and LV-TGFβ2 eyes at night ($P < 0.01$). These data indicate that i) TRPV4
219 activation is necessary for OHT in the TGFβ2 overexpression mouse model (Figures 5-6) and the
220 circadian IOP elevations ii) TGFβ2 -evoked OHT does not affect nocturnal IOP elevation in mice, and iii)
221 TRPV4 inhibition does not disrupt the mechanisms that maintain daytime normotensive IOP (Figures 5-
222 6).

223 **Discussion**

224 The mechanistic framework developed in this study unifies key biochemical and biomechanical
225 risk factors of POAG to point towards an alternative approach to mitigate fibrotic and functional
226 dysfunction in eyes experiencing OHT. Specifically, we show that TGFβ2 drives overexpression and
227 excessive activation of TRPV4, a Ca^{2+}-permeable channel with diverse mechanosensing functions that
228 include mediating the principal component of the pressure-activated transmembrane current roles in TM
229 cells and fibrotic remodeling across the body (39, 68, 69). Our central observation - that tonic TRPV4
230 activity is obligatory to maintain TM contractility and OHT induced by angle occlusion and TGFβ2 –
231 identifies a potential molecular linchpin for increased resistance of the JCT TM to AH outflow.
232 Considering that current glaucoma treatments target secondary outflow mechanisms or are associated
233 with side effects (such as hyperemia) (70, 71), the IOP lowering effected by TRPV4 inhibition and gene
234 knockdown suggests a novel target within the primary outflow pathway that can be engaged without
235 compromising the structural integrity or function of the anterior eye.

Glaucoma is a multifactorial disease with etiology that reflects the convergence of risk factors that include IOP and TGFβ2: the likelihood of POAG correlates with the amplitude of IOP and $[TGF\beta2]_{AH}$ (22, 72), and chronic increases in either $[TGF\beta2]_i$ or IOP promote fibrotic remodeling of the TM/SC and augment the AH flow resistance of the conventional pathway (17, 24, 25). TGFβ2-induced facility suppression has been historically attributed to changes in composition, crosslinking and amount of ECM (25, 26, 73, 74), activation of Hippo signaling and Rho kinase- (Rho/ROCK) mediated contractility (19, 57) and altered expression of genes encoding mitogen-activated protein kinase (MAPK), immune response, oxidative stress, and/or ECM pathways (75–77). Our discovery that TGFβ2 impacts the expression and function of TM mechanosensors and *vice versa*, that TRPV4 is required for TGFβ2-induced contractility, coalesces two key modifiable risk factors (TGFβ2 and pressure) at the level of TRPV4 signaling. Specifically, our data embed TGFβ2 and TRPV4 signaling within reciprocal feedback loops: TGFβ2 (i) induced time-dependent upregulation of TRPV4 mRNA and protein and amplified TRPV4-mediated calcium signaling, while (ii) TRPV4 was required to mediate TGFβ2 -induced contractility and maintain chronic OHT in TGFβ2-treated mouse eyes. Microinjection of the selective antagonist HC-06 accordingly reduced IOP in LV- TGFβ2-treated eyes to baseline with hypotension persisting for ~4 days and reversing to pre-injection OHT by day 7. The TRPV4-dependence of TGFβ2-induced OHT and contractility was validated *in vivo* using *Trpv4*$^{-/-}$ eyes and *in vitro* in 3D hydrogel constructs. The differential effectiveness of IOP lowering induced by gene knockdown (~50% reduction in OHT) and pharmacological inhibition (~100% reduction in OHT) may reflect compensatory upregulation of cognate mechanosensory mechanisms in *Trpv4*$^{-/-}$ animals (55).

We've previously shown that TRPV4 channels in primary human TM cells are activated by physiological (5 – 25 mm Hg) pressure steps (39, 60) and (1 – 12%) strains (37, 41), to activate downstream outflow-relevant signaling mechanisms such as Rho kinase, F-actin, tyrosine phosphorylation of FAK, paxillin and vinculin, reorganization of membrane lipids, and ECM release (37, 41, 52). Here, we extend those observations to demonstrate that TRPV4 activation is required for TM

contractility and ocular hypertension induced by TGFβ2 overexpression and circadian rhythmicity. The observation that TRPV4 activity underpins increased outflow resistance under physiological and pathological conditions resolves contradictory conclusions from prior investigations, which implicated TRPV4 signaling in ocular hypertension and hypotension, respectively (7, 36, 37, 39, 41, 52, 53, 55). TRPV4 has been proposed to lower IOP through phosphoinositide signaling in primary cilia (36), stimulate TM-resident endothelial nitric oxide synthase (eNOS) (7) and release of polyunsaturated fatty acids (PUFAs) (53) and/or activate downstream from Piezo1 mechanosensing (54). However, TRPV4-regulated Ca^{2+} influx in TM cells is unaffected by the ablation of primary cilia (37), eNOS expression in TM cells is vanishingly low (78–80), PUFAs such as arachidonic acid and EETs stimulate rather than inhibit, TRPV4 (37) and TRPV4 signaling in TM cells is unaffected by Piezo1 inhibitors and knockdown (39). Moreover, Piezo1 inhibition reduces outflow facility under *in vitro* and *in vivo* conditions (39, 81), indicating opposing homeostatic functions for Piezo1 vs. TRPV4 activation. The TRPV4-dependence of TM contractility (Figure 4) accords with reports that TRPV4 inhibition increases, and TRPV4 activation reduces outflow facility in biomimetic TM-populated scaffolds in the absence of ciliary body, Schlemm's canal, and ciliary muscle (37). Induction of the contractile response by GSK101 and its inhibition of hypercontractility by HC-06 further suggest a model whereby TRPV4 pressure transduction drives Ca^{2+}- and Rho-dependent hypercontractility and fibrosis via actin polymerization, myosin light chain phosphorylation, aSMA integration into stress fibers and reinforcement of focal ECM contacts (41, 82, 83) (Figure 7). TRPV4 channels in cells treated with TGFβ2 are likely to be constitutively active at incubator temperature, which coincides with peak TRPV4 thermoactivation (~34 - 37^{o}C) (84, 85). The residual contractility in HC-06-treated cells may reflect TGFβ2-mediated contributions from Piezo1, TRPC, and/or TREK-1 channels and/or intracellular Ca^{2+} release (37, 60, 86, 87). Reports from heart, lung, liver, skin and articular cartilage preparations similarly implicate TRPV4 in TGFβ1 -dependent fibrosis (68, 88–91) and bladder (92), heart (93, 94), and vascular (95) contractility, with conditional ablation of TRPV4 from smooth muscle cells shown to lower blood pressure (96, 97). TGFβ2-stimulated induction of *FN1*, *SNAIL1*, and *CTGF* transcripts (Figure 1) accords with RNA profiling studies which

documented the cytokine's key role in TM transdifferentiation towards the contractile myofibroblast state (25, 75, 98–103) whereas the decreased expression of TGFBR2 and increased the abundance of SMAD7 mRNA indicate activation of autoinhibitory mechanisms in EMT -undergoing cells (104).

Treatment of TM cells with TGFβ2 concentrations comparable to those found in POAG AH (0.2-3.2 ng/ml) (20) produced 2-3-fold upregulation of TRPV4 transcripts, protein, and responsiveness to GSK101, with the time course of these effects mirroring facility reduction in human eyes treated with exogenous cytokine (105). A single exposure to 5 ng/ml TGFβ2 approximately doubled the amplitude of the GSK101-evoked current and reduced outward rectification of I_{TRPV4} (Figure 3). Difficulties with giga-ohm seal formation precluded I_{TRPV4} analyses at longer incubation times but we were able to obviate this limitation with imaging experiments, which revealed robust and reproducible time-dependent increases in the amplitude of agonist-induced Ca^{2+} signals across all 5 studied strains (Figure 2). The effects of TGFβ2 on I_{TRPV4}, membrane protein levels and $[Ca^{2+}]_{GSK}$ accord with increased expression of the TRPV4 gene, with precedents from other cell types (e.g., fibroblasts) suggesting the possibility of increased trafficking of TRPV4- PI3Kg complexes and/or β-arrestin 1-dependent ubiquitination (106, 107). The upregulation of TRPV4/Piezo1 transcription predicts that TGFβ2-exposed cells might exhibit exaggerated responsiveness to mechanical loading and mechanical hyperalgesia, as reported for chemotherapy (108), neuropathic pain (109, 110), cancer (111), and diabetic neuropathy (112).

The lack of additivity between TGFβ2-induced OHT and nocturnal OHT (Figure 6) suggests that control of physiological and pathological hypertension converges at the level of TRPV4-Rho signaling as the final common mechanism obligatory for OHT. This conjecture is supported by the observations that TRPV4 inhibitors, ROCK inhibitors and TM-specific expression of dominant negative scAAV2.*dnRhoA* constructs lower IOP, elevated through occlusion of the iridocorneal angle, TGFβ, glucocorticoids and the nocturnal cycle (55, 62, 113). Future studies of TRPV4 signaling will investigate the mechanisms that underlie the reversibility of circadian TRPV4 activation and how TGFβ2 impairs this physiological process. For example, the suprachiasmatic nucleus and the hypothalamus–pituitary–adrenal axis (114,

115) may modulate the TRPV4-Rho axis via nocturnal release of norepinephrine and melatonin (116, 117). It is worth noting that TRPV4 may directly bind to membrane proteins known to regulate conventional outflow, such as β1 integrins (118), caveolin-1 (52), and cytoskeletal proteins (actin, actin adaptor proteins, microtubules) (119).

Our study unifies biomechanical and biochemical paradigms of fibrotic and functional remodeling in glaucoma, expands the biological significance of TGFβ2 modulation by including increased actomyosin contractility in addition to fibrotic remodeling, thereby opening a new window into the mechanisms that subserve physiological vs. pathological OHT. We propose that TGFβ2 shifts the homeostatic normotensive setpoint maintained by steady-state TRPV4, Piezo1 and TREK-1 activation (39, 60, 81) through upregulation of TRPV4 expression, which increases the cells' sensitivity to pressure and strain under normotensive conditions. In addition to hijacking the cells' contractile apparatus, TGFβ2 overexposure induces fibrosis that may facilitate the pull of stress fibers on the increasingly "stiff" ECM (19) together with increased production and secretion of ECM. The absence of structural and functional visual phenotypes in TRPV4 KO mice (55, 66, 120) predicts that small-molecule TRPV4 antagonists might lower IOP, suppress fibrosis and protect retinal neurons without compromising homeostatic IOP regulation (70). The similarities between TRPV4 expression in mouse and human TM (37) and between outflow mechanisms in mice vs. humans (121, 122) suggest that TRPV4 targeting might be explored within the clinical context.

Methods

Animals

C57BL/6J mice were from JAX laboratories (Bar Harbor, ME), *Trpv4*$^{-/-}$ mice were a gift from Wolfgang Liedtke (Duke University) (64, 65). The animals were maintained in a pathogen-free facility with a 12-hour light/dark cycle and ad libitum access to food and water, at a temperature of ~22-23°C. Mice were 2-

6 months in age prior to LV-injection; data from both male and female sexed animals were included in this study.

Human TM Culture

De-identified postmortem eyes from donors with no history of glaucoma (pTM cells) were procured from Utah Lions Eye Bank with written informed consent of the donor's families. TM cells were isolated from juxtacanalicular and corneoscleral regions as previously described (37, 39), in accordance with consensus characterization recommendations (123). pTM cells were cultured in Trabecular Meshwork Cell Medium (TMCM; Sciencell) in Collagen-I (Corning) coated culture flasks and glass coverslips at 37°C in a humidified atmosphere with 5% CO2. Fresh media was supplied every 2-3 days. Serum free (SF) media was mixed as needed by excluding fetal bovine serum (FBS, Sciencell) from the TMCM. A list of all pTM strains used is available in Table 1; all cells were used between passages 2-4. Cell lines were chosen based on availability at the time of experiments.

For contractility experiments pTM cells were isolated from healthy donor corneal rims discarded after transplant surgery, as previously described (19, 57, 124), and cultured according to established protocols (123, 125). Three pTM cell strains isolated from healthy donors and validated with dexamethasone-induced myocilin expression were used for contractility experiments. pTM cells were cultured in low-glucose Dulbecco's Modified Eagle's Medium (DMEM; Gibco; Thermo Fisher Scientific) containing 10% fetal bovine serum (FBS; Atlanta Biologicals) and 1% penicillin/streptomycin/glutamine (PSG; Gibco) and maintained at 37°C in a humidified atmosphere with 5% CO2. Fresh media was supplied every 2-3 days.

The experiments were conducted according to the tenets of the Declaration of Helsinki for the use of human tissue.

Reagents

The TRPV4 antagonist HC-067047 (HC-06) was purchased from Millipore-Sigma or Cayman Biotech and dissolved in DMSO at 20mM. The TRPV4 agonist GSK1016790A (GSK101; Cayman Biotech) was dissolved in DMSO at 1mM. Aliquots were diluted into working concentrations (10-25 nM, GSK101; 5-100 µM, HC-06). Recombinant human TGFβ2 protein was ordered from R&D Systems and reconstituted in sterile 4 mM HCl with 0.1% BSA at 20 ug/mL.

Quantitative Real-Time PCR

Gene-specific primers were used to detect expression of target genes, as described (126). Total RNA was isolated using the Arcturus PicoPure RNA isolation kit (Thermofisher Scientific). cDNA was generated from total RNA using qScript XLT cDNA Supermix (Quanta Biosciences). SYBR Green based real-time PCR was performed with 2X GREEN Master Mix (Apex Bioresearch Products). Gapdh was used as an endogenous control to normalize fluorescence signals. Gene expression relative to GAPDH was measured using the comparative CT method ($2^{-[\Delta CT(gene)- \Delta CT(GAPDH)]}$). All genes were assessed in 4-8 individual samples taken from 3-7 different pTM strains. The primer sequences, expected product length, and gene accession are given in Table 2.

Western Blot

3 SF- or TGFβ2-treated samples were pelleted and pooled together from 3 different pTM samples within the same condition. To separate membrane proteins from heavier cellular debris the pooled cell pellets were homogenized in a hypotonic lysis buffer (20mM TRIS-HCl, 3mM MgCl2, 10mM NaCl, 10mM PMSF, 0.5 mM DTT, 20 mM NaF, 2 mM NaV, 0.5 µg/mL leupeptin) before centrifuging at 300x g for 5 minutes (4 °C). The resulting supernatant was removed and centrifuged again at >12,500 rpm for 30 minutes to pellet membrane proteins, which were then resuspended in RIPA Buffer (Santa Cruz). Proteins were separated on a 10% SDS-PAGE gel and transferred to polyvinylidene difluoride membranes (Bio-Rad). Membranes were blocked with 5% skim milk/2% BSA in TBST and incubated at 4 °C overnight with a primary antibody against TRPV4 (1:250, Alomone Labs #ACC-034) or rabbit antibody against β-

tubulin (1:2000, Abcam #EPR1330). Appropriate secondary antibodies conjugated to HRP were used to visualize protein expression on an iBright CL750 imaging system (Thermo Fisher Scientific). β-Tubulin expression was used to standardize protein levels between samples.

Calcium Imaging

pTM cells were seeded onto Collagen-I (Corning) coated coverslips and cultured in TMCM media (ScienCell) as described (39, 41). The cells were serum starved for 24 hours followed by serum-free TMCM with or without TGFβ2 (1 or 5 ng/mL) for 24 hours or five days. The cells were loaded with 10 μM of the ratiometric indicator Fura-2 AM (K_d at RT = 225 nM (Invitrogen/ThermoFisher) for 30-60 minutes. Coverslips were placed in a RC-26G chamber platform (Warner Instrument Corp) and perfused with external saline (pH 7.4) (in mM): 80 NaCl, 4.7 KCl, 1.2 MgCl2, 10 D-Glucose, 19.1 HEPES sodium salt, 2 $CaCl_2$ and osmolality adjusted to 300 mOsm using D-mannitol. External solutions were delivered via a manually controlled gravity-fed eight-line manifold system, with perfusion speed kept constant to minimize changes in shear. Epifluorescence imaging was performed using an inverted Nikon Ti microscope with a 40x 1.3 N.A. oil objective and Nikon Elements AR software. 340 nm and 380 nm excitation were delivered by a high-intensity 150W Xenon arc lamp (Lambda DG-4; Sutter Instruments), high pass-filtered at 510 nm and detected with a 12-bit Delta Evolve camera (Photometrics/Teledyne). GSK101 (10 nM) evoked $\Delta[Ca^{2+}]_i$ was assessed as ΔR/R (dividing the difference between the peak GSK-evoked F_{340}/F_{380} signal during stimulation and baseline F_{340}/F_{380} signal by the baseline F_{340}/F_{380} signal). Every data point represents a separate experimental day and pTM cell strain, each with 3-5 control and 3-5 TGFβ2-treated slides tested on the same day. TGFβ2 datapoints represent the average GSK101 evoked ΔR/R across all TGFβ2 cells as a % of the average ΔR/R of control cells from the same cell strain on the same day.

Collagen hydrogel contraction assay

Rat tail collagen type I (Corning, Thermo Fisher Scientific) was prepared at a concentration of 1.5 mg/ml according to the manufacturer's instructions. Five hundred microliters of the hydrogel solution were pipetted into 24-well culture plates. Upon complete collagen polymerization, pTM cells were seeded at 1.5 × 105 cells/well atop the hydrogels and cultured in DMEM + 10% FBS + 1% PSG for 48 hours to facilitate even cell spreading. Next, constructs were cultured in serum-free DMEM + 1% PSG supplemented with: i) control (vehicle: 0.008 mM HCl + 0.0004% BSA; 0.025% DMSO), ii) TGFβ2 (5 ng/ml; R&D Systems), or iii and iv) TGFβ2 + HC067047 (5 μM in DMSO) for 36 hours before carefully releasing the hydrogels from the walls using a sterile 10 μl pipette tip to facilitate contraction. The next morning, fresh serum-free DMEM + 1% PSG supplemented with 0.0025% DMSO (= vehicle) was added to groups i-iii; group iv received serum-free DMEM + 1% PSG supplemented with GSK1016790A (25 nM in DMSO). Plates were longitudinally imaged at 600 dpi resolution with a CanoScan LiDE 300 flatbed scanner (Canon USA) at 0, 15, 30, 60, and 120 minutes. Hydrogel construct size was quantified using FIJI software (National Institutes of Health) (127).

Electrophysiology

Borosilicate patch-clamp pipettes (WPI) were pulled using a P-2000 horizontal micropipette puller (Sutter Instruments), with a resistance of 6-8 MΩ. The internal solution contained (mM): 125 K-gluconate, 10 KCl, 1.5 MgCl2, 10 HEPES, 10 EGTA, pH 7.4. Patch clamp data was acquired with a Multiclamp 700B amplifier, pClamp 10.6 software and Digidata 1440A interface (Molecular Devices), sampled at 5kHz and analyzed with Clampfit 10.7. Current-voltage relationships were assessed using V_m steps from -100 to + 100 mV against a holding potential of -30 mV. Current density was measured as the average current during GSK101 exposure subtracted by the average current from the same cell during baseline perfusion.

IOP Measurements

A TonoLab rebound tonometer (Colonial Medical Supply) was used to measure IOP of awake mice between 12-2 P.M. IOP was determined from the mean of 10-20 tonometer readings. Nocturnal

measurements were conducted between 9-10 P.M. under 2.5% isoflurane delivered by a Somnosuite isoflurane vaporizer (Kent Scientific). After animals recovered from intracameral HC-06/PBS injections, IOP was measured daily. IOP was measured every day for 4-5 consecutive days to confirm a stable return to baseline. IOP data for individual cohorts was binned into weeks of experimental time to group values for analysis.

Lentiviral Transduction

Lentiviral stock for TGFβ2 (C226,228S) was purchased from VectorBuilder Inc. (VB170816-1094fnw, pLV[Exp]-CMV> {hTGFB2[NM_003238.3](C226,228S)}) (23). Scrambled control lentivirus was purchased from SignaGen Laboratories (LM-CMV-Null-Puro). Mice were anesthetized with an intraperitoneal IP injection of ketamine/xylazine (90 mg/10 mg/ kg body weight), followed by eyedrops containing 0.5% proparacaine hydrochloride and 1% tropicamide ophthalmic solution to numb the eyes and dilate the pupils. Anesthetized mice were secured to allow stereotaxic injection of lentivirus. Intravitreal injections were conducted by creating a guide hole with a 30-gauge needle 1-2 mm equatorial of the cornea-scleral border followed by insertion of a 12° beveled 33-gauge Hamilton syringe (Hamilton Company) secured to a stereotaxic rig (World Precision Instruments) used to insert the needle 2-3 mm into the eye. Each eye was injected with a 2uL bolus of lentivirus diluted to $1x10^6$ TU/µL over the course of one minute, before the needle was quickly drawn and the pilot hole treated with erythromycin ophthalmic ointment USP (Bausch & Lomb). The efficiency of LV-TGFβ2 OHT induction in WT animals was close to 100%. No differences in observable health post-injection were detected between wild type and *Trpv4*$^{-/-}$ animals or LV-Ctrl and LV-TGFβ2 injected animals.

Intracameral Microinjections

Mice were anesthetized and treated with eyedrops as above, before being placed on an isothermal heating pad. HC-06 (100 µM) or PBS with DMSO (0.5%) as a vehicle were injected into the anterior chamber using a blunt tip Hamilton syringe (Hamilton Company) through a guide hole made using a 30-gauge

454 needle. At the end of each injection a small air bubble was introduced to seal the cornea and minimize
455 fluid outflow. 0.5% Erythromycin ophthalmic ointment USP (Bausch & Lomb) was applied to the eye
456 after the procedure. Intracameral injections were not associated with observable inflammation, corneal
457 opacity or behavioral changes. For the nocturnal IOP experiments in Figure 6, two animals were injected
458 with PBS while two were injected with HC-06. When OHT was stably reestablished a week post-
459 injection, the treatment groups were switched, and experiments repeated to obtain four eyes/treatment
460 group for Figure 6*C-D*.

461 Statistical Analysis

462 GraphPad Prism 9 was used for statistical analysis. Means are plotted ± SEM unless otherwise noted.
463 One-sample t-tests were used to determine whether TGFβ2 treated groups were significantly different
464 than untreated control groups, while one-way ANOVA or two-way ANOVA along with Tukey or
465 Bonferroni's multiple comparisons test were used to compare multiple groups.

466 Study Approval

467 The animal experimental protocols were conducted in accordance with the NIH Guide for the Care and
468 Use of Laboratory Animals and the ARVO Statement for the Use of Animals in Ophthalmic and Vision
469 Research and were approved by the Institutional Animal Care and Use Committee at the University of
470 Utah.

471 Data Availability

472 Individual datapoints for in-vivo figures, and unedited/uncropped annotated western blot images, are
473 included in the supplementary data files for this manuscript. Further information about the data presented
474 in this manuscript is available from the corresponding authors upon reasonable request.

475 **Author Contributions**

476 C.N.R. and D.K. designed the primary research study. C.N.R., M.L., A.S., S.N.R., D.K., Y.T.T., M.L.

performed research, C.N.R., S.N.R., Y.T.T., S.H., D.K. analyzed the data, and C.N.R. and D.K. wrote the paper.

Acknowledgements & Funding

We thank Dr. Paloma Liton (Duke University) for the generous gift of LV-TGFβ2^{C226,228S} lentivirus stock during the pilot stages of this experiment, and Dr. Gulab Zode for the availability of the LV-TGFβ2^{C226,228S} construct on Vectorbuilder. We additionally thank Dr. Wolfgang Liedtke (Duke University and Regeneron) for *Trpv4*$^{-/-}$ mice.

The study was supported by the National Institutes of Health (T32EY024234 to CNR and DK, R01EY022076, R0EY1031817, P30EY014800 to DK, R01EY034096 to SH, R01EY022359, R01EY005722 to WDS), Crandall Glaucoma Initiative, Stauss-Rankin Foundation, and Unrestricted Grants from Research to Prevent Blindness to Ophthalmology Departments at the University of Utah and Duke University.

References

1. Y. C. Tham, *et al.*, Global prevalence of glaucoma and projections of glaucoma burden through 2040: A systematic review and meta-analysis. *Ophthalmology* **121**, 2081–2090 (2014).

2. M. O. Gordon, *et al.*, The Ocular Hypertension Treatment Study: Baseline factors that predict the onset of primary open-angle glaucoma. *Arch. Ophthalmol.* **120**, 714–720 (2002).

3. A. Heijl, *et al.*, Reduction of intraocular pressure and glaucoma progression: Results from the Early Manifest Glaucoma Trial. *Arch. Ophthalmol.* **120**, 1268–1279 (2002).

4. M. Almasieh, A. M. Wilson, B. Morquette, J. L. Cueva Vargas, A. Di Polo, The molecular basis of retinal ganglion cell death in glaucoma. *Prog. Retin. Eye Res.* **31**, 152–181 (2012).

5. C. Baudouin, M. Kolko, S. Melik-Parsadaniantz, E. M. Messmer, Inflammation in Glaucoma: From the back to the front of the eye, and beyond. *Prog. Retin. Eye Res.* **83** (2021).

6. B. A. Ellingsen, W. M. Grant, The relationship of pressure and aqueous outflow in enucleated human eyes. *Invest. Ophthalmol.* **10**, 430–437 (1971).

7. P. D. Patel, *et al.*, Impaired TRPV4-eNOS signaling in trabecular meshwork elevates intraocular pressure in glaucoma. *Proc. Natl. Acad. Sci. U. S. A.* **118** (2021).

8. A. W. De Kater, A. Shahsafaei, D. L. Epstein, Localization of smooth muscle and nonmuscle actin isoforms in the human aqueous outflow pathway. *Investig. Ophthalmol. Vis. Sci.* **33**, 424–429 (1992).

9. David Krizaj, "No cell is an island: trabecular meshwork ion channels as sensors of the ambient milieu" in *Glaucoma Research and Clinical Advances: 2020 to 2022*, Vol. 3, J. R. Samples, P. A. Knepper, Eds. (Kugler Publications, 2020), pp. 1–10.

10. J. M. Baumann, *et al.*, TRPV4 and chloride channels mediate volume sensing in trabecular meshwork cells. *Am. J. Physiol. Physiol.* (2024). https://doi.org/10.1152/ajpcell.00295.2024.

11. R. F. Brubaker, The effect of intraocular pressure on conventional outflow resistance in the enucleated human eye. *Invest. Ophthalmol.* **14**, 286–292 (1975).

12. A. Karimi, *et al.*, The Effect of Intraocular Pressure Load Boundary on the Biomechanics of the Human Conventional Aqueous Outflow Pathway. *Bioengineering* **9** (2022).

13. T. Borrás, Gene expression in the trabecular meshwork and the influence of intraocular pressure. *Prog. Retin. Eye Res.* **22**, 435–463 (2003).

14. R. F. Ramos, G. M. Sumida, W. Daniel Stamer, Cyclic mechanical stress and trabecular meshwork cell contractility. *Investig. Ophthalmol. Vis. Sci.* **50**, 3826–3832 (2009).

15. C. Luna, G. Li, P. B. Liton, D. L. Epstein, P. Gonzalez, Alterations in gene expression induced by cyclic mechanical stress in trabecular meshwork cells. *Mol. Vis.* **15**, 534–544 (2009).

16. T. S. Acott, J. A. Vranka, K. E. Keller, V. K. Raghunathan, M. J. Kelley, Normal and glaucomatous outflow regulation. *Prog. Retin. Eye Res.* **82** (2021).

17. R. Fuchshofer, E. R. Tamm, The role of TGF-β in the pathogenesis of primary open-angle glaucoma. *Cell Tissue Res.* **347**, 279–290 (2012).

18. M. A. Johnstone, Intraocular pressure regulation: Findings of pulse-dependent trabecular meshwork motion lead to unifying concepts of intraocular pressure homeostasis. *J. Ocul. Pharmacol. Ther.* **30**, 88–93 (2014).

19. H. Li, V. K. Raghunathan, W. D. Stamer, P. S. Ganapathy, S. Herberg, Extracellular Matrix Stiffness and TGFβ2 Regulate YAP/TAZ Activity in Human Trabecular Meshwork Cells. *Front. Cell Dev. Biol.* **10** (2022).

20. P. Agarwal, A. M. Daher, R. Agarwal, Aqueous humor TGF-β2 levels in patients with open-angle glaucoma: A meta-analysis. *Mol. Vis.* **21**, 612–620 (2015).

21. Y. Ochiai, H. Ochiai, Higher concentration of transforming growth factor-β in aqueous humor of glaucomatous eyes and diabetic eyes. *Jpn. J. Ophthalmol.* **46**, 249–253 (2002).

22. R. C. Tripathi, J. Li, W. F. A. Chan, B. J. Tripathi, Aqueous humor in glaucomatous eyes contains an increased level of TGF-β2. *Exp. Eye Res.* **59**, 723–728 (1994).

23. S. V. Patil, R. B. Kasetti, J. C. Millar, G. S. Zode, A Novel Mouse Model of TGFβ2-Induced Ocular Hypertension Using Lentiviral Gene Delivery. *Int. J. Mol. Sci.* **23** (2022).

24. A. R. Shepard, *et al.*, Adenoviral gene transfer of active human transforming growth factor-β2 elevates intraocular pressure and reduces outflow facility in rodent eyes. *Investig. Ophthalmol. Vis. Sci.* **51**, 2067–2076 (2010).

25. D. L. Fleenor, *et al.*, TGFβ2-induced changes in human trabecular meshwork: Implications for intraocular pressure. *Investig. Ophthalmol. Vis. Sci.* **47**, 226–234 (2006).

26. M. Montecchi-Palmer, *et al.*, TGFβ2 induces the formation of cross-linked actin networks (CLANs) in human trabecular meshwork cells through the smad and non-smad dependent pathways. *Investig. Ophthalmol. Vis. Sci.* **58**, 1288–1295 (2017).

27. R. K. Coker, *et al.*, Transforming growth factors-β1, -β2, and -β3 stimulate fibroblast procollagen production in vitro but are differentially expressed during bleomycin-induced lung fibrosis. *Am. J. Pathol.* **150**, 981–991 (1997).

28. B. Santiago, *et al.*, Topical application of a peptide inhibitor of transforming growth factor-β1 ameliorates bleomycin-induced skin fibrosis. *J. Invest. Dermatol.* **125**, 450–455 (2005).

29. Y. Yue, K. Meng, Y. Pu, X. Zhang, Transforming growth factor beta (TGF-β) mediates cardiac fibrosis and induces diabetic cardiomyopathy. *Diabetes Res. Clin. Pract.* **133**, 124–130 (2017).

30. Y. Zhang, *et al.*, Overexpression of TGF-b1 induces renal fibrosis and accelerates the decline in kidney function in polycystic kidney disease. *Am. J. Physiol. - Ren. Physiol.* **319**, F1135–F1148 (2020).

31. M. Walker, M. Godin, A. E. Pelling, Mechanical stretch sustains myofibroblast phenotype and function in microtissues through latent TGF-β1 activation. *Integr. Biol.* **12**, 199–210 (2020).

32. P. J. Wipff, D. B. Rifkin, J. J. Meister, B. Hinz, Myofibroblast contraction activates latent TGF-β1 from the extracellular matrix. *J. Cell Biol.* **179**, 1311–1323 (2007).

33. G. Zhen, *et al.*, Mechanical stress determines the configuration of TGFβ activation in articular cartilage. *Nat. Commun.* **12** (2021).

34. N. E. Cabrera-Benítez, *et al.*, Mechanical stress induces lung fibrosis by epithelial-mesenchymal transition. *Crit. Care Med.* **40**, 510–517 (2012).

35. S. C. Wei, J. Yang, Forcing through Tumor Metastasis: The Interplay between Tissue Rigidity and Epithelial-Mesenchymal Transition. *Trends Cell Biol.* **26**, 111–120 (2016).

36. N. Luo, *et al.*, Primary cilia signaling mediates intraocular pressure sensation. *Proc. Natl. Acad. Sci. U. S. A.* **111**, 12871–12876 (2014).

37. D. A. Ryskamp, *et al.*, TRPV4 regulates calcium homeostasis, cytoskeletal remodeling, conventional outflow and intraocular pressure in the mammalian eye. *Sci. Rep.* **6** (2016).

38. Y. F. Yang, Y. Y. Sun, D. M. Peters, K. E. Keller, The Effects of Mechanical Stretch on Integrins and Filopodial-Associated Proteins in Normal and Glaucomatous Trabecular Meshwork Cells. *Front. Cell Dev. Biol.* **10** (2022).

39. O. Yarishkin, *et al.*, Piezo1 channels mediate trabecular meshwork mechanotransduction and promote aqueous fluid outflow. *J. Physiol.* **599**, 571–592 (2021).

40. J. P. M. White, *et al.*, TRPV4: Molecular conductor of a diverse orchestra. *Physiol. Rev.* **96**, 911–973 (2016).

41. M. Lakk, D. Krizaj, TRPV4-Rho signaling drives cytoskeletal and focal adhesion remodeling in trabecular meshwork cells. *Am. J. Physiol. - Cell Physiol.* **320**, C1013–C1030 (2021).

42. V. Katari, N. Bhavnani, S. Paruchuri, C. Thodeti, TRPV4 regulates matrix stiffness-dependent activation of YAP/VEGFR2 signaling via Rho/Rho kinase/LATS1/2 pathway. *FASEB J.* **35** (2021).

43. B. Nilius, T. Voets, The puzzle of TRPV4 channelopathies. *EMBO Rep.* **14**, 152–163 (2013).

44. M. L. Thibodeau, *et al.*, Compound heterozygous TRPV4 mutations in two siblings with a complex phenotype including severe intellectual disability and neuropathy. *Am. J. Med. Genet. Part A* **173**, 3087–3092 (2017).

45. C. J. Klein, *et al.*, TRPV4 mutations and cytotoxic hypercalcemia in axonal Charcot-Marie-Tooth neuropathies. *Neurology* **76**, 887–894 (2011).

46. Z. Daneva, *et al.*, Caveolar peroxynitrite formation impairs endothelial TRPV4 channels and elevates pulmonary arterial pressure in pulmonary hypertension. *Proc. Natl. Acad. Sci. U. S. A.* **118** (2021).

47. O. Pochynyuk, O. Zaika, R. G. O'Neil, M. Mamenko, Novel insights into TRPV4 function in the kidney. *Pflugers Arch. Eur. J. Physiol.* **465**, 177–186 (2013).

48. M. W. G. Roberts, *et al.*, TRPV4 receptor as a functional sensory molecule in bladder urothelium: Stretch-independent, tissue-specific actions and pathological implications. *FASEB J.* **34**, 263–286 (2020).

49. K. Shibasaki, TRPV4 activation by thermal and mechanical stimuli in disease progression. *Lab. Investig.* **100**, 218–223 (2020).

50. T. L. Toft-Bertelsen, *et al.*, Lysophosphatidic acid as a CSF lipid in posthemorrhagic hydrocephalus that drives CSF accumulation via TRPV4-induced hyperactivation of NKCC1. *Fluids Barriers CNS* **19** (2022).

51. L. Lapajne, *et al.*, TRPV4: Cell type-specific activation, regulation and function in the vertebrate eye. *Curr. Top. Membr.* **89**, 189–219 (2022).

52. M. Lakk, *et al.*, Membrane cholesterol regulates TRPV4 function, cytoskeletal expression, and the cellular response to tension. *J. Lipid Res.* **62** (2021).

53. T. Uchida, *et al.*, TRPV4 is activated by mechanical stimulation to induce prostaglandins release in trabecular meshwork, lowering intraocular pressure. *PLoS One* **16** (2021).

54. L. Jing, K. Liu, F. Wang, Y. Su, Role of mechanically-sensitive cation channels Piezo1 and TRPV4 in trabecular meshwork cell mechanotransduction. *Hum. Cell* **37**, 394–407 (2024).

55. S. N. Redmon, *et al.*, TRPV4 subserves physiological and pathological elevations in intraocular pressure. *Res. Sq. [Preprint]* (2024). https://doi.org/10.21203/rs.3.rs-4714050/v1.

56. A. Nettesheim, M. S. Shim, J. Hirt, P. B. Liton, Transcriptome analysis reveals autophagy as regulator of TGFβ/Smad-induced fibrogenesis in trabecular meshwork cells. *Sci. Rep.* **9** (2019).

57. H. Li, J. L. Henty-Ridilla, A. M. Bernstein, P. S. Ganapathy, S. Herberg, TGFβ2 Regulates Human Trabecular Meshwork Cell Contractility via ERK and ROCK Pathways with Distinct Signaling Crosstalk Dependent on the Culture Substrate. *Curr. Eye Res.* **47**, 1165–1178 (2022).

58. X. Yan, X. Xiong, Y. G. Chen, Feedback regulation of TGF-β signaling. *Acta Biochim. Biophys. Sin. (Shanghai).* **50**, 37–50 (2018).

59. T. Carreon, E. van der Merwe, R. L. Fellman, M. Johnstone, S. K. Bhattacharya, Aqueous outflow - A continuum from trabecular meshwork to episcleral veins. *Prog. Retin. Eye Res.* **57**, 108–133 (2017).

60. O. Yarishkin, *et al.*, TREK-1 channels regulate pressure sensitivity and calcium signaling in trabecular meshwork cells. *J. Gen. Physiol.* **150**, 1660–1675 (2018).

61. M. Honjo, *et al.*, Effects of protein kinase inhibitor, HA1077, on intraocular pressure and outflow facility in rabbit eyes. *Arch. Ophthalmol.* **119**, 1171–1178 (2001).

62. P. V. Rao, P. P. Pattabiraman, C. Kopczynski, Role of the Rho GTPase/Rho kinase signaling pathway in pathogenesis and treatment of glaucoma: Bench to bedside research. *Exp. Eye Res.* **158**, 23–32 (2017).

63. C. R. Ethier, A. T. Read, D. W. H. Chan, Effects of latrunculin-B on outflow facility and trabecular meshwork structure in human eyes. *Investig. Ophthalmol. Vis. Sci.* **47**, 1991–1998 (2006).

64. W. Liedtke, J. M. Friedman, Abnormal osmotic regulation in trpv4-/- mice. *Proc. Natl. Acad. Sci. U. S. A.* **100**, 13698–13703 (2003).

65. D. A. Ryskamp, *et al.*, The polymodal ion channel transient receptor potential vanilloid 4

modulates calcium flux, spiking rate, and apoptosis of mouse retinal ganglion cells. *J. Neurosci.* **31**, 7089–7101 (2011).

66. O. Yarishkin, T. T. T. Phuong, M. Lakk, D. Križaj, TRPV4 does not regulate the distal retinal light response. *Adv. Exp. Med. Biol.* **1074**, 553–560 (2018).

67. K. Ikegami, S. Masubuchi, Suppression of trabecular meshwork phagocytosis by norepinephrine is associated with nocturnal increase in intraocular pressure in mice. *Commun. Biol.* **5** (2022).

68. S. O. Rahaman, *et al.*, TRPV4 mediates myofibroblast differentiation and pulmonary fibrosis in mice. *J. Clin. Invest.* **124**, 5225–5238 (2014).

69. V. P. Willard, *et al.*, Transient receptor potential vanilloid 4 as a regulator of induced pluripotent stem cell chondrogenesis. *Stem Cells* **39**, 1447–1456 (2021).

70. N. A. Sharif, Identifying new drugs and targets to treat rapidly elevated intraocular pressure for angle closure and secondary glaucomas to curb visual impairment and prevent blindness. *Exp. Eye Res.* **232** (2023).

71. R. N. Weinreb, C. B. Toris, B. T. Gabelt, J. D. Lindsey, P. L. Kaufman, Effects of prostaglandins on the aqueous humor outflow pathways. *Surv. Ophthalmol.* **47** (2002).

72. M. C. Leske, *et al.*, Factors for glaucoma progression and the effect of treatment: The early manifest glaucoma trial. *Arch. Ophthalmol.* **121**, 48–56 (2003).

73. R. Fuchshofer, M. Birke, U. Welge-Lussen, D. Kook, E. Lütjen-Drecoll, Transforming growth factor-β2 modulated extracellular matrix component expression in cultured human optic nerve head astrocytes. *Investig. Ophthalmol. Vis. Sci.* **46**, 568–578 (2005).

74. W. E. Medina-Ortiz, R. Belmares, S. Neubauer, R. J. Wordinger, A. F. Clark, Cellular fibronectin expression in human trabecular meshwork and induction by transforming growth factor-β2. *Investig. Ophthalmol. Vis. Sci.* **54**, 6779–6788 (2013).

75. B. Callaghan, *et al.*, Genome-wide transcriptome profiling of human trabecular meshwork cells treated with TGF-β2. *Sci. Rep.* **12** (2022).

76. M. Inoue-Mochita, *et al.*, P38 MAP kinase inhibitor suppresses transforming growth factor-β2-induced type 1 collagen production in trabecular meshwork cells. *PLoS One* **10** (2015).

77. M. H. Kang, D. J. Oh, J. heon Kang, D. J. Rhee, Regulation of SPARC by transforming growth factor β2 in human trabecular meshwork. *Investig. Ophthalmol. Vis. Sci.* **54**, 2523–2532 (2013).

78. G. Patel, *et al.*, Molecular taxonomy of human ocular outflow tissues defined by single-cell transcriptomics. *Proc. Natl. Acad. Sci. U. S. A.* **117**, 12856–12867 (2020).

79. E. Reina-Torres, *et al.*, The vital role for nitric oxide in intraocular pressure homeostasis. *Prog. Retin. Eye Res.* **83** (2021).

80. T. van Zyl, *et al.*, Cell atlas of aqueous humor outflow pathways in eyes of humans and four model species provides insight into glaucoma pathogenesis. *Proc. Natl. Acad. Sci. U. S. A.* **117**, 10339–10349 (2020).

81. W. Zhu, *et al.*, The role of Piezo1 in conventional aqueous humor outflow dynamics. *iScience* **24** (2021).

82. P. P. Pattabiraman, *et al.*, Rhoa gtpase-induced ocular hypertension in a rodent model is associated with increased fibrogenic activity in the trabecular meshwork. *Am. J. Pathol.* **185**, 496–512 (2015).

83. M. Zhang, R. Maddala, P. V. Rao, Novel molecular insights into RhoA GTPase-induced resistance to aqueous humor outflow through the trabecular meshwork. *Am. J. Physiol. - Cell Physiol.* **295** (2008).

84. A. D. Güler, *et al.*, Heat-evoked activation of the ion channel, TRPV4. *J. Neurosci.* **22**, 6408–6414 (2002).

85. R. Nishimoto, *et al.*, Thermosensitive TRPV4 channels mediate temperature-dependent microglia movement. *Proc. Natl. Acad. Sci. U. S. A.* **118** (2021).

86. E. Abad, *et al.*, Activation of store-operated Ca2+ channels in trabecular meshwork cells. *Investig. Ophthalmol. Vis. Sci.* **49**, 677–686 (2008).

87. M. Feger, *et al.*, The production of fibroblast growth factor 23 is controlled by TGF-andbeta. *Sci. Rep.* **7** (2017).

88. S. Sharma, *et al.*, TRPV4 ion channel is a novel regulator of dermal myofibroblast differentiation. *Am. J. Physiol. - Cell Physiol.* **312**, C562–C572 (2017).

89. R. K. Adapala, *et al.*, TRPV4 channels mediate cardiac fibroblast differentiation by integrating mechanical and soluble signals. *J. Mol. Cell. Cardiol.* **54**, 45–52 (2013).

90. C. J. O'Conor, H. A. Leddy, H. C. Benefield, W. B. Liedtke, F. Guilak, TRPV4-mediated mechanotransduction regulates the metabolic response of chondrocytes to dynamic loading. *Proc. Natl. Acad. Sci. U. S. A.* **111**, 1316–1321 (2014).

91. Y. Songa, *et al.*, TRPV4 channel inhibits TGF-β1-induced proliferation of hepatic stellate cells. *PLoS One* **9** (2014).

92. Y. Wu, J. Qi, C. Wu, W. Rong, Emerging roles of the TRPV4 channel in bladder physiology and dysfunction. *J. Physiol.* **599**, 39–47 (2021).

93. J. L. Jones, *et al.*, TRPV4 increases cardiomyocyte calcium cycling and contractility yet contributes to damage in the aged heart following hypoosmotic stress. *Cardiovasc. Res.* **115**, 46–56 (2019).

94. S. Chaigne, S. Barbeau, T. Ducret, R. Guinamard, D. Benoist, Pathophysiological Roles of the TRPV4 Channel in the Heart. *Cells* **12** (2023).

95. X. Wen, *et al.*, Aortic smooth muscle TRPV4 channels regulate vasoconstriction in high salt-induced hypertension. *Hypertens. Res.* **46**, 2356–2367 (2023).

96. Y. L. Chen, *et al.*, Novel Smooth Muscle Ca2+-Signaling Nanodomains in Blood Pressure Regulation. *Circulation* **146**, 548–564 (2022).

97. Y. Zhu, *et al.*, Vascular Smooth Muscle TRPV4 (Transient Receptor Potential Vanilloid Family Member 4) Channels Regulate Vasoconstriction and Blood Pressure in Obesity. *Hypertension* **80**, 757–770 (2023).

98. X. Zhao, K. E. Ramsey, D. A. Stephan, P. Russell, Gene and protein expression changes in human trabecular meshwork cells treated with transforming growth factor-β. *Investig. Ophthalmol. Vis. Sci.* **45**, 4023–4034 (2004).

99. A. Zhavoronkov, *et al.*, Pro-fibrotic pathway activation in trabecular meshwork and lamina cribrosa is the main driving force of glaucoma. *Cell Cycle* **15**, 1643–1652 (2016).

100. J. A. Last, *et al.*, Elastic modulus determination of normal and glaucomatous human trabecular meshwork. *Investig. Ophthalmol. Vis. Sci.* **52**, 2147–2152 (2011).

101. U. Raychaudhuri, J. C. Millar, A. F. Clark, Tissue transglutaminase elevates intraocular pressure in mice. *Investig. Ophthalmol. Vis. Sci.* **58**, 6197–6211 (2017).

102. A. T. Read, D. W. H. Chan, C. R. Ethier, Actin structure in the outflow tract of normal and glaucomatous eyes. *Exp. Eye Res.* **84**, 214–226 (2007).

103. K. Wang, A. T. Read, T. Sulchek, C. R. Ethier, Trabecular meshwork stiffness in glaucoma. *Exp. Eye Res.* **158**, 3–12 (2017).

104. R. Fuchshofer, D. A. Stephan, P. Russell, E. R. Tamm, Gene expression profiling of TGFβ2- and/or BMP7-treated trabecular meshwork cells: Identification of Smad7 as a critical inhibitor of TGF-β2 signaling. *Exp. Eye Res.* **88**, 1020–1032 (2009).

105. J. Gottanka, D. Chan, M. Eichhorn, E. Lütjen-Drecoll, C. R. Ethier, Effects of TGF-β2 in Perfused Human Eyes. *Investig. Ophthalmol. Vis. Sci.* **45**, 153–158 (2004).

106. L. M. Grove, *et al.*, Translocation of TRPV4-PI3Kγ complexes to the plasma membrane drives myofibroblast transdifferentiation. *Sci. Signal.* **12** (2019).

107. A. K. Shukla, *et al.*, Arresting a transient receptor potential (TRP) channel: β-arrestin 1 mediates ubiquitination and functional down-regulation of TRPV4. *J. Biol. Chem.* **285**, 30115–30125 (2010).

108. Y. Matsumura, *et al.*, The prophylactic effects of a traditional Japanese medicine, goshajinkigan, on paclitaxel-induced peripheral neuropathy and its mechanism of action. *Mol. Pain* **10** (2014).

109. Y. Zhang, *et al.*, A transient receptor potential vanilloid 4 contributes to mechanical allodynia following chronic compression of dorsal root ganglion in rats. *Neurosci. Lett.* **432**, 222–227 (2008).

110. N. Alessandri-Haber, O. A. Dina, E. K. Joseph, D. Reichling, J. D. Levine, A transient receptor potential vanilloid 4-dependent mechanism of hyperalgesia is engaged by concerted action of inflammatory mediators. *J. Neurosci.* **26**, 3864–3874 (2006).

111. A. Maqboul, B. Elsadek, Expression profiles of TRPV1, TRPV4, TLR4 and ERK1/2 in the dorsal root ganglionic neurons of a cancer-induced neuropathy rat model. *PeerJ* **2018** (2018).

112. Y. Y. Cui, *et al.*, Expression and functional characterization of transient receptor potential vanilloid 4 in the dorsal root ganglion and spinal cord of diabetic rats with mechanical allodynia. *Brain Res. Bull.* **162**, 30–39 (2020).

113. T. Borrás, L. K. Buie, M. G. Spiga, J. Carabana, Prevention of nocturnal elevation of intraocular pressure by gene transfer of dominant-negative RhoA in rats. *JAMA Ophthalmol.* **133**, 182–190 (2015).

114. B. C. Samuels, *et al.*, Dorsomedial/perifornical hypothalamic stimulation increases intraocular pressure, intracranial pressure, and the translaminar pressure gradient. *Investig. Ophthalmol. Vis. Sci.* **53**, 7328–7335 (2012).

115. K. Ikegami, Circadian rhythm of intraocular pressure. *J. Physiol. Sci.* **74**, 14 (2024).

116. K. Z. Shen, R. A. North, A. Surprenant, Potassium channels opened by noradrenaline and other transmitters in excised membrane patches of guinea-pig submucosal neurones. *J. Physiol.* **445**, 581–599 (1992).

117. E. A. Steinberg, K. A. Wafford, S. G. Brickley, N. P. Franks, W. Wisden, The role of K2P channels in anaesthesia and sleep. *Pflugers Arch. Eur. J. Physiol.* **467**, 907–916 (2015).

118. B. D. Matthews, *et al.*, Ultra-rapid activation of TRPV4 ion channels by mechanical forces applied to cell surface β1 integrins. *Integr. Biol.* **2**, 435–442 (2010).

119. C. Goswami, J. Kuhn, P. A. Heppenstall, T. Hucho, Importance of non-selective cation channel TRPV4 interaction with cytoskeleton and their reciprocal regulations in cultured cells. *PLoS One* **5** (2010).

120. A. O. Jo, *et al.*, Differential volume regulation and calcium signaling in two ciliary body cell types is subserved by TRPV4 channels. *Proc. Natl. Acad. Sci. U. S. A.* **113**, 3885–3890 (2016).

121. A. Boussommier-Calleja, *et al.*, Pharmacologic manipulation of conventional outflow facility in ex vivo mouse eyes. *Investig. Ophthalmol. Vis. Sci.* **53**, 5838–5845 (2012).

122. D. R. Overby, *et al.*, The structure of the trabecular meshwork, its connections to the ciliary muscle, and the effect of pilocarpine on outflow facility in mice. *Investig. Ophthalmol. Vis. Sci.* **55**, 3727–3736 (2014).

123. K. E. Keller, *et al.*, Consensus recommendations for trabecular meshwork cell isolation, characterization and culture. *Exp. Eye Res.* **171**, 164–173 (2018).

124. T. Bagué, *et al.*, Effects of Netarsudil-Family Rho Kinase Inhibitors on Human Trabecular Meshwork Cell Contractility and Actin Remodeling Using a Bioengineered ECM Hydrogel. *Front. Ophthalmol.* **2** (2022).

125. W. D. Stamer, R. E. B. Seftor, S. K. Williams, H. A. M. Samaha, R. W. Snyder, Isolation and culture of human trabecular meshwork cells by extracellular matrix digestion. *Curr. Eye Res.* **14**, 611–617 (1995).

126. T. T. T. Phuong, *et al.*, Calcium influx through TRPV4 channels modulates the adherens contacts between retinal microvascular endothelial cells. *J. Physiol.* **595**, 6869–6885 (2017).

127. J. Schindelin, *et al.*, Fiji: An open-source platform for biological-image analysis. *Nat. Methods* **9**, 676–682 (2012).

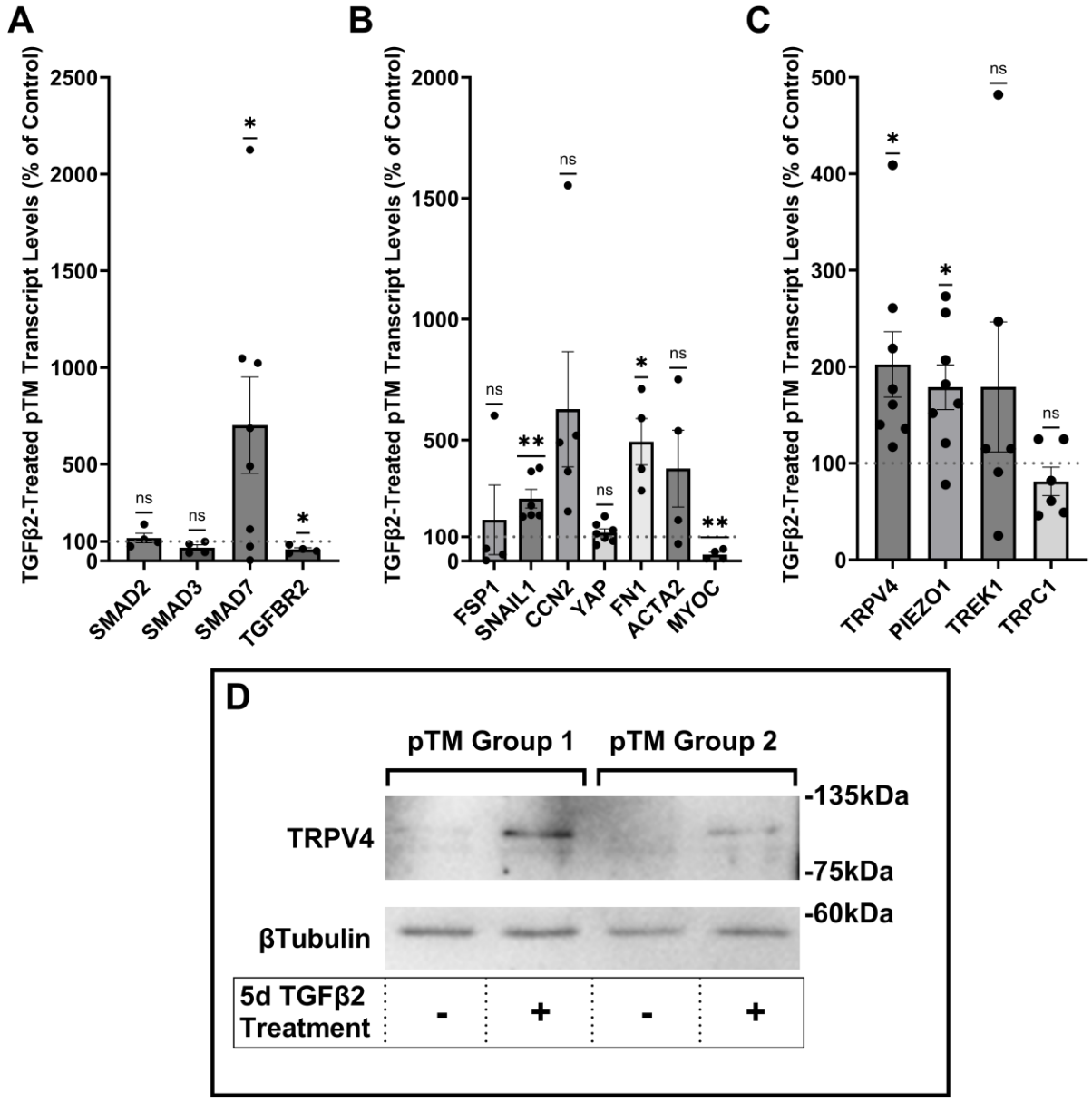

Figure 1: TGFβ2 induces a fibrotic phenotype in pTM cells and increases expression and membrane insertion of the TRPV4 channel.

(**A**-**B**) Five-day TGFβ2 treatment (1ng/mL) significantly altered expression of TGFβ pathway effectors, cytoskeletal machinery, and canonical fibrotic markers. (**C**) TGFβ2 treatment significantly increased *TRPV4* and *PIEZO1* expression, but not *TREK1* and *TRPC1* expression. Mean ± SEM shown. N = 4 - 8 experiments, each gene tested in 3-7 different pTM strains (See Table 1). Two-tailed one sample t-test of TGFβ2-induced gene expression levels as a percent of control samples. (**D**) Isolation of membrane proteins from two separate pooled pTM samples suggests TGFβ2 treatment drives increased TRPV4 membrane insertion. N = 2 independent pooled samples, 3 pTM strains were pooled per sample. * $P < 0.05$, ** $P < 0.01$.

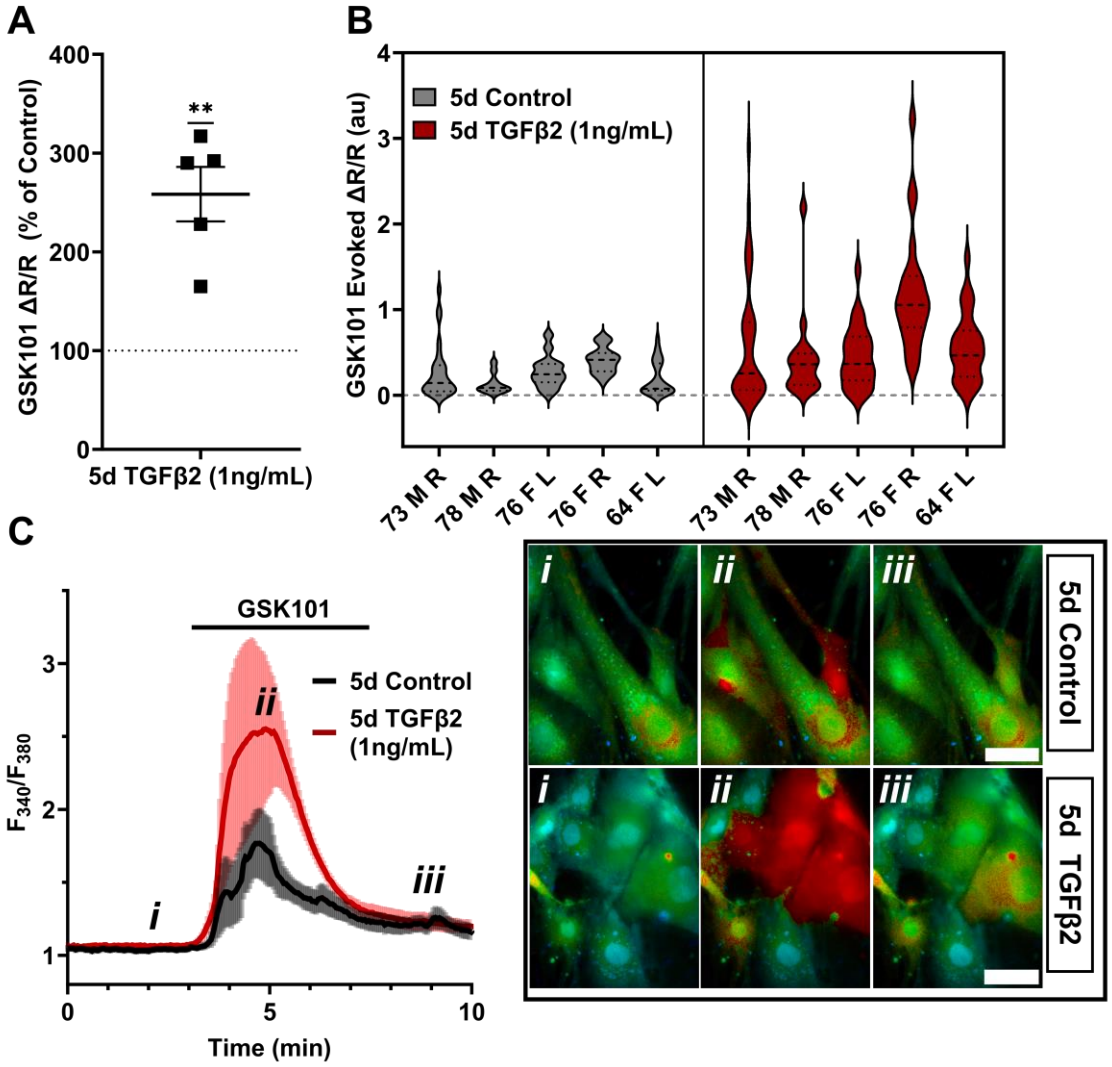

802

803 **Figure 2: TRPV4-mediated Ca^{2+} influx is potentiated by five-day TGFβ2 treatment.**

804 (**A**) Five-day TGFβ2 treatment (1 ng/mL) increased TRPV4 agonist-induced (GSK101, 10 nM) Ca^{2+}
805 influx in pTM cells compared to serum-free media alone treated cells tested on the same day (N = 5 pTM
806 strains, n = 3 - 5 slides/condition/day, individual data points over mean ± SEM). Two-tailed one sample t-
807 test of TGFβ2-treated cell average GSK101 response as a percent of control samples from the same pTM
808 strain on the same day. (**B**) Violin plots showing the distribution of GSK101-induced Ca^{2+} responses for
809 each pTM strain tested in A. Thick dashed line indicates mean, while light dashed line indicates quartiles.
810 (**C**) Representative traces showing TRPV4 agonist-induced Ca^{2+} influx (seen as an increase in F_{340}/F_{380}) in
811 pTM (mean ± SEM of 4 representative cells/ group), alongside example Fura-2-loaded pTM cells before
812 (i), during (ii), and after (iii) GSK101 application. Scale bar = 50 µm. ** $P < 0.01$

813

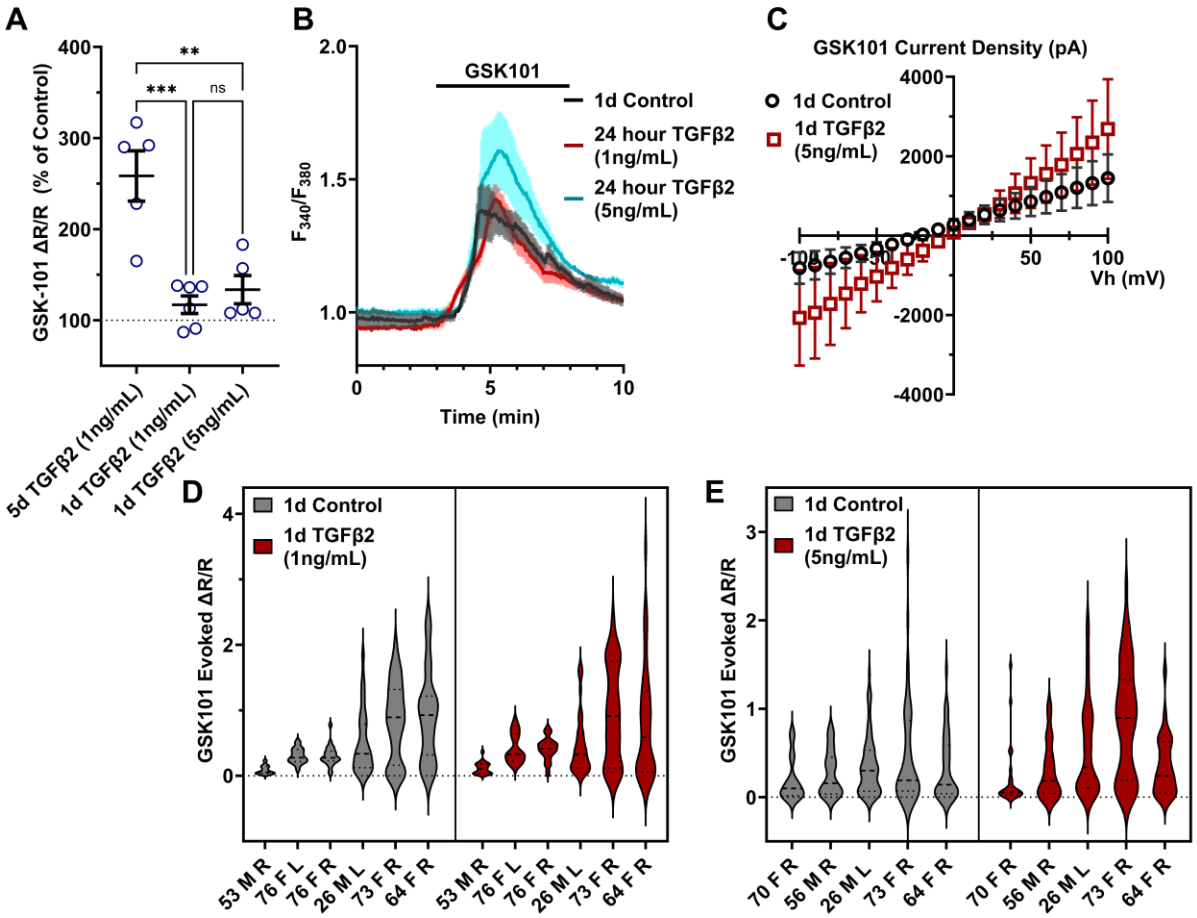

Figure 3: TGFB2-induced TRPV4 potentiation is not seen at a shorter time period, regardless of treatment strength.

(**A**) TGFβ2 treatments for 24 hours at 1 ng/mL (N = 6 pTM strains, n = 3 - 5 slides/condition/day) or 5 ng/mL (N = 5 pTM strains, n = 3 - 5 slides/condition/day) did not show potentiation of GSK101-evoked TRPV4 Ca^{2+} influx (SI Appendix, Figure S1) and were significantly lower than cells treated with TGFβ2 for 5d at 1ng/mL (5d TGFβ2 results from Figure 2A). Individual data points over mean ± SEM. One-way ANOVA with Tukey's multiple comparisons test, statistics for individual 1d treatment groups compared to control groups shown in Figure S1. (**B**) Representative traces for GSK101 response following 24-hour TGFβ2 treatment, traces show mean ± SEM of 3-4 cells. (**C**) Average current density in response to GSK101 (24-hour control: n = 11 cells, 24-hour TGFβ2: n=10 cells) shows generally increased current in TGFβ2-treated cells. Data shows mean ± SEM (**D - E**) Violin plots of individual cell strains shown in **A**. Thick dashed line indicates mean, while light dashed line indicates quartiles. ** $P < 0.01$, *** $P < 0.001$

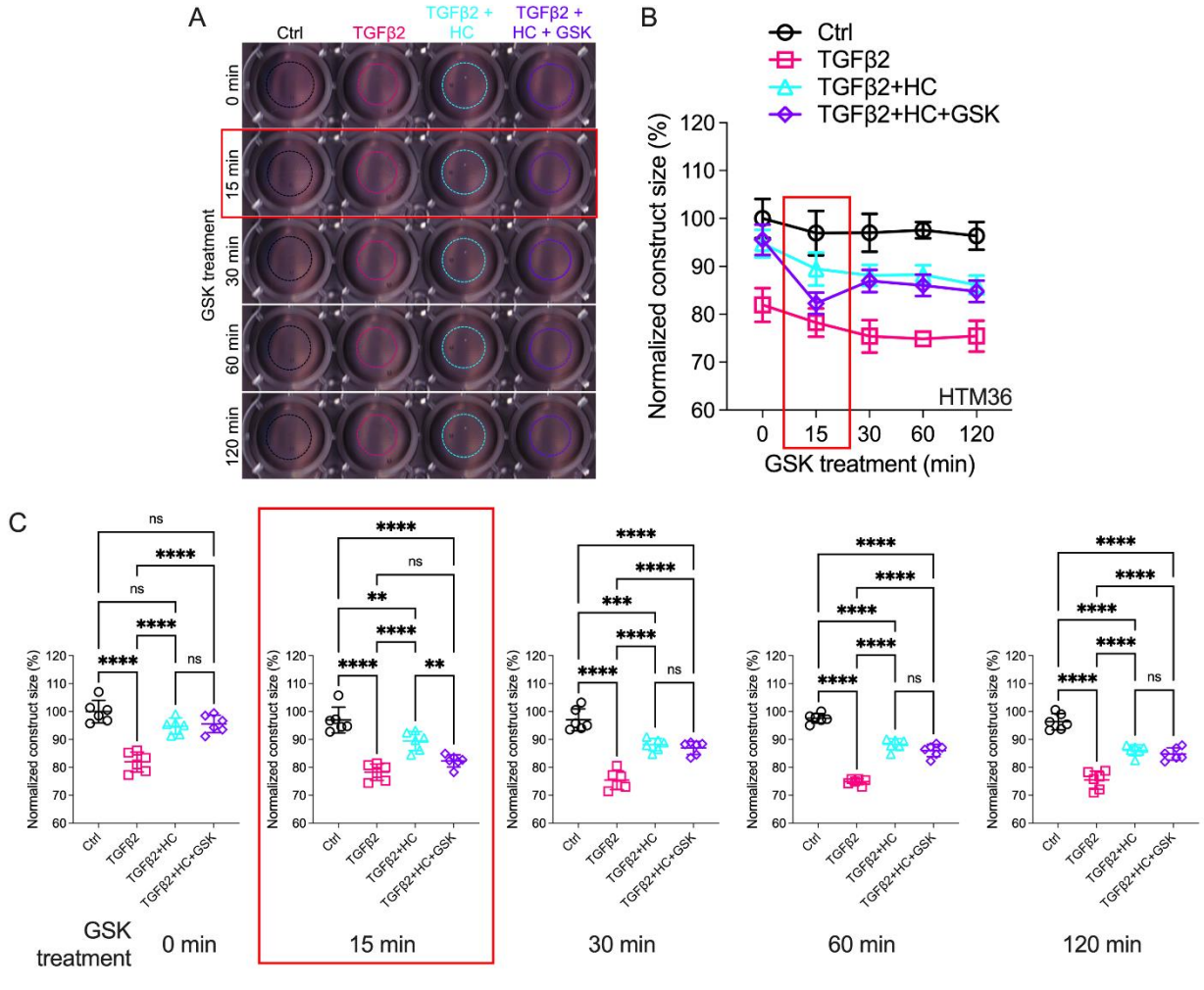

Figure 4: Effects of TRPV4 inhibition/activation on TGFβ2-induced contraction of TM cells. (**A**) Representative longitudinal 24-well plate scans of collagen type I hydrogels seeded with pTM subjected to the different treatments (dashed lines outline size of contracted constructs). (**B**) Longitudinal quantification of hydrogel construct size compared to the control group at the 0 minute time point. (**C**) Detailed comparisons between groups at each experimental time point. n = 6 hydrogels/group. One-way ANOVA with Tukey's multiple comparisons test, data in (**B,D**) shows individual data points over mean ± S.D. One pTM strain shown: TGFβ2-induced contractility induction, HC-06-mediated rescue of hypercontractility, and GSK101-induced transient (15 min) contraction were consistent across (3/3) pTM strains tested (Figure S2). ** $P < 0.01$, *** $P < 0.001$, **** $P < 0.0001$.

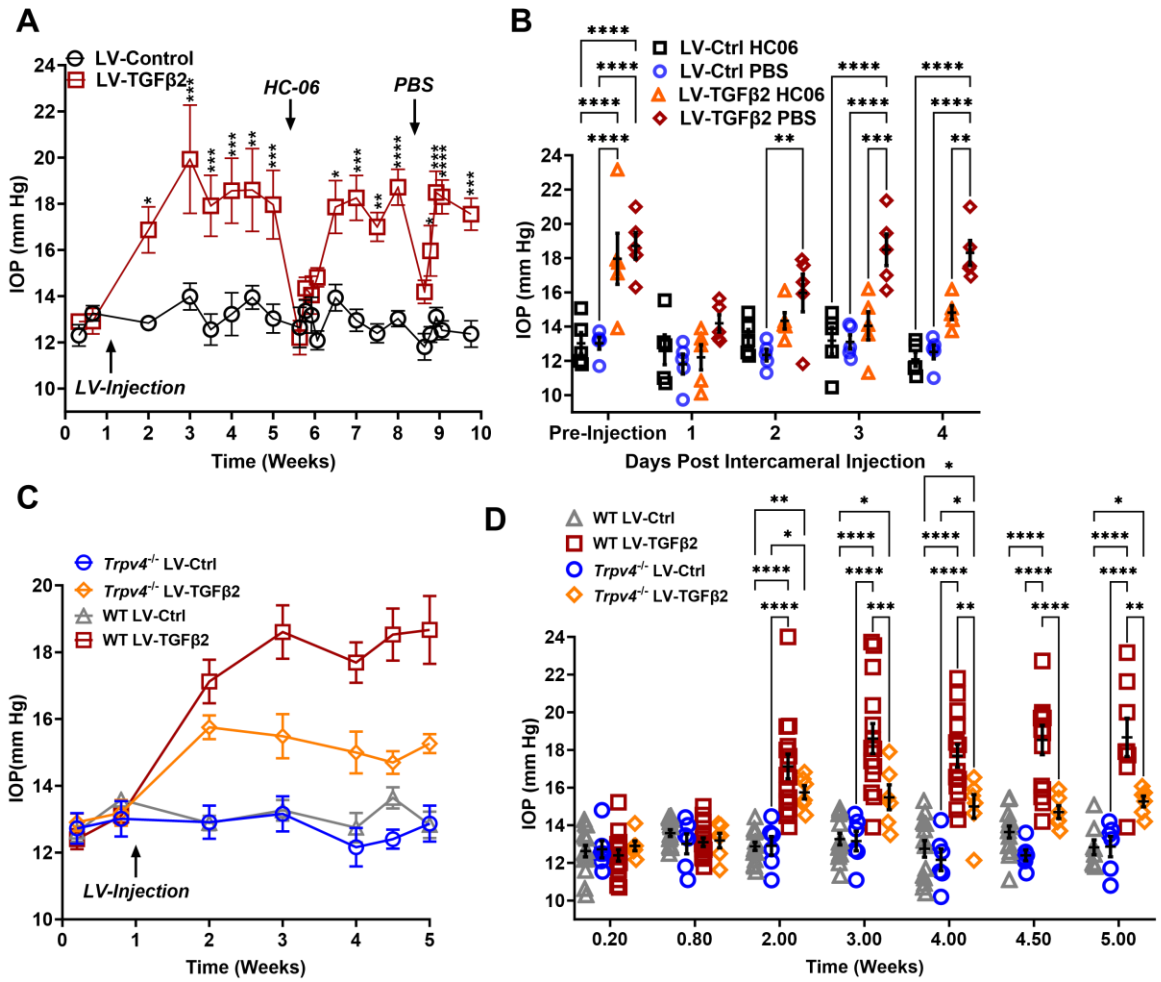

Figure 5: TRPV4 activation is necessary to maintain LV-TGFβ2-induced ocular hypertension. (**A**) Intravitreal injection of LV-TGFβ2 (week 1), but not LV-Control, elevates IOP in WT mice (N = 5 eyes/group) as early as one-week post-injection. Injection of TRPV4 antagonist HC-06, but not PBS, produced multiday IOP reduction in LV-TGFβ2 treated eyes. HC-06 and PBS injections did not affect IOP in LV-Control injected eyes. Two-way ANOVA with Bonferroni post-hoc analysis (**B**) Direct comparison of the results of PBS and HC-06 injections in the eyes shown in **A**. Two-way ANOVA with Bonferroni post-hoc analysis (**C**) Intravitreal injection of LV-TGFβ2 in *Trpv4*$^{-/-}$ mice (N = 6 eyes/group) resulted in only mild OHT; plotted against WT eyes at matching timepoints (3 WT cohorts including the 5 WT eyes shown in A-B, N = 8-15 eyes/group). (**D**) Statistical comparison of the IOP values shown in **C.** The IOP in LV-TGFβ2 WT eyes was significantly elevated compared to the LV-TGFβ2 *Trpv4*$^{-/-}$ eyes from 2 weeks post-injection. LV-Control injected eyes in WT or *Trpv4*$^{-/-}$ eyes remain close to the baseline value and are not significantly different. Two-way ANOVA with Bonferroni post-hoc analysis. (**A, C)** shows mean ± SEM**.** Data in (**B, D**) shows individual data points over mean ± SEM, * $P < 0.05$, ** $P < 0.01$, *** $P < 0.001$, **** $P < 0.0001$

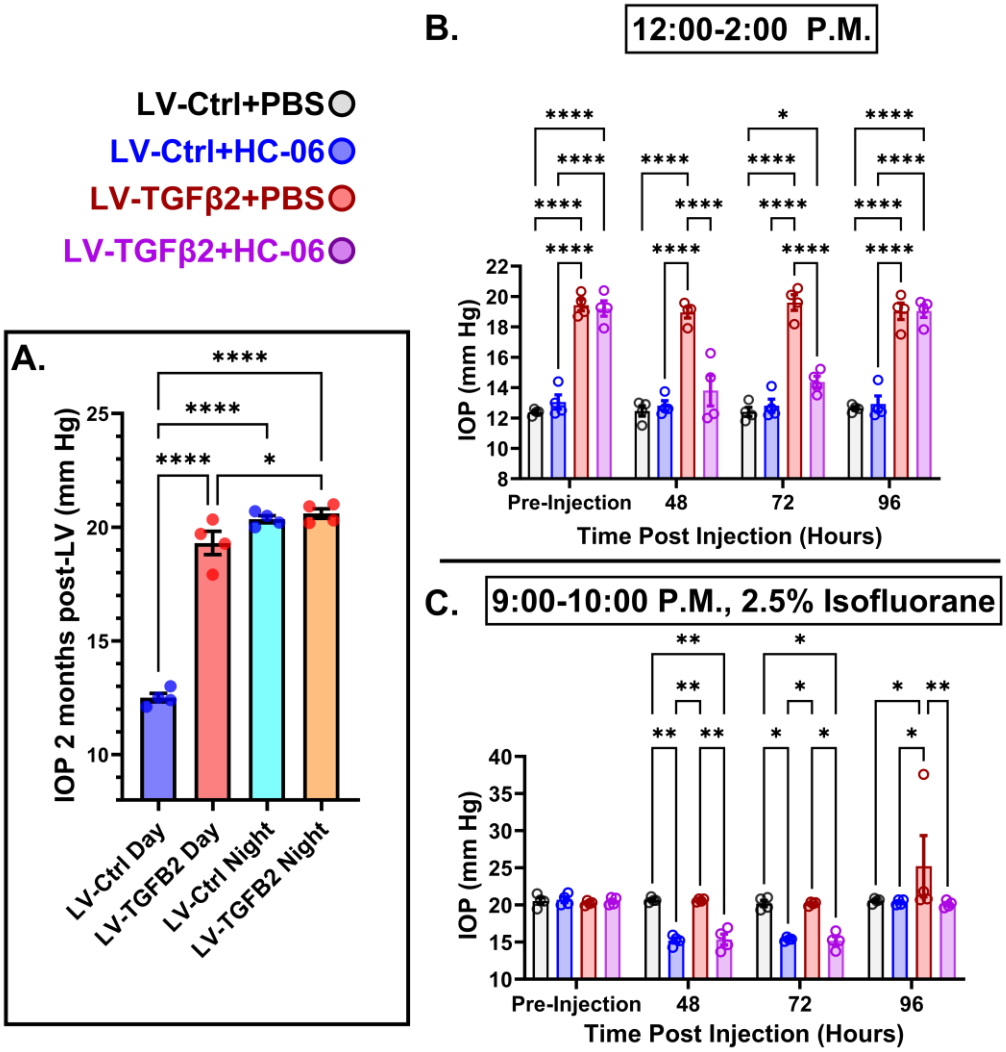

Figure 6: TRPV4 inhibition inhibits nocturnal IOP elevation in control and TGFβ2 overexpressing eyes. (**A**) ~2 months post-LV injection daytime (12-2:00 P.M) and nocturnal (9-10:00 P.M.) IOP compared in WT mice (N = 4 eyes/group) before drug treatment. LV-TGFβ2 eyes were elevated at daytime, but nocturnal OHT was not significantly different between LV-Ctrl and LV-TGFβ2 eyes. One-way ANOVA with Tukey's multiple comparisons test. (**B-C)** PBS-injected eyes did not exhibit changes in daytime or nighttime intraocular pressure; however, HC-06 injection reduced TGFβ2-induced IOP elevations during the day and LV-Ctrl and LV-TGFβ2 nocturnal IOPs (N = 4 Eyes/Group); Two-way ANOVA with Bonferroni post-hoc analysis. Figures show datapoints over mean ± SEM, *$P < 0.05$, ** $P < 0.01$, *** $P < 0.001$, **** $P < 0.0001$

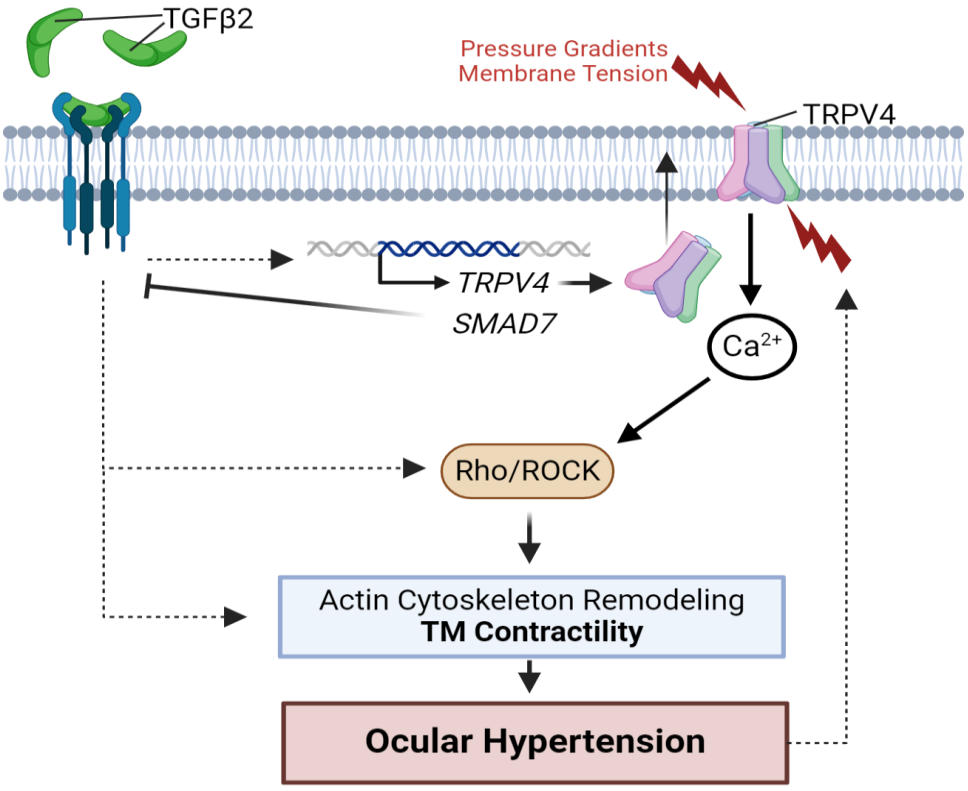

Figure 7: TGFβ2-TRPV4 interactions in TM remodeling and ocular hypertension. Chronic exposure to TGFβ2 induces upregulation of functional TRPV4 channels alongside the autoinhibitory canonical modulator SMAD7. TRPV4-mediated Ca^{2+} influx, canonical, and non-canonical TGFβ2 signaling stimulate Rho/ROCK signaling, augment cytoskeletal contractility, and stimulate ECM release to increase the flow resistance of the conventional pathway. Increased contractility drives OHT, resulting in a feedforward vicious TRPV4-dependent circle loop that maintains ocular hypertension. Schematic made using Biorender.com.

875

876

Location	Donor Age	Donor Sex	Experiments Used
Utah	55	M	PCR, Electrophysiology
Utah	76 (a)	F	PCR, WB, Ca^{2+} Img.
Utah	76 (b)	F	PCR, Ca^{2+} Img.
Utah	78	M	PCR, Ca^{2+} Img.
Utah	64 (a)	F	PCR, WB, Ca^{2+} Img.
Utah	64 (b)	F	PCR, Ca^{2+} Img.
Utah	70 (a)	F	PCR, WB, Ca^{2+} Img., Electrophysiology
Utah	70 (b)	F	PCR
Utah	53	M	Ca^{2+} Img.
Utah	26	M	Ca^{2+} Img., Electrophysiology
Utah	73	F	Ca^{2+} Img.
Utah	56	M	Ca^{2+} Img.
Utah	73	M	Ca^{2+} Img.
Utah	80	M	WB
SUNY	39	M	Contractility
SUNY	50	F	Contractility
SUNY	56	F	Contractility

877 **Table 1: Donor information for primary human trabecular meshwork (pTM) strains used in this**

878 **study.**

879

880

Gene	Forward	Reverse	Product Length (bp)	NCBI reference number
GAPDH	CTCCTGTTCGACAGTCAGCC	GACTCCGACCTTCACCTTCC	89	NM_002046.5
SMAD2	GGGTTTTGAAGCCGTCTATCAGC	CCAACCACTGTAGAGGTCCATTC	149	NM_005901.6
SMAD3	CAAGTGGCCGCGTGTAAAAA	AGTCCAGAACAGCCGAGTTG	181	NM_005902.4
SMAD7	CTGCTCCCATCCTGTGTGTT	CCTTGGGTTATGACGGACCA	120	NM_005904.3
TGFBR2	AACCTCTAGGCACCCTCCTC	AACCTCTAGGCACCCTCCTC	100	NM_001024847.3
FSP1	GCTTCTTCTTTCTTGGTTTGATCCT	AAGTCCACCTCGTTGTCCCT	250	NM_002961.3
SNAIL1	GGCTCCTTCGTCCTTCTCCTCTAC	CTGGAGATCCTTGGCCTCAGAGAG	124	NM_005985.4
CCN2	CCCCAGACACTGGTTTGAAG	CCCACTGCTCCTAAAGCCAC	100	NM_001901.3
YAP1	ACAGGGAAGTGACTTTGTACA	GCACTGAATATTGCACCCAC	183	NM_001130145.
FN1	CTGAAAGACCAGCAGAGGCA	GTGTAGGGGTCAAAGCACGA	110	M10905.1
SMA (ACTA2)	GTCACCCACAATGTCCCCAT	GGAATAGCCACGCTCAGTCA	123	NM_001141945.2
MYOC	CCACGTGGAGAATCGACACA	TCCAGTGGCCTAGGCAGTAT	118	NM_000261.1
TRPV4	TCCCATTCTTGCTGACCCAC	AGGGCTGTCTGACCTCGATA	217	NM_021625.4
PIEZO1	GGCCAACTTCCTCACCAAGA	GGGTATTTCTTCTCTGTCTC	106	NM_001142864.3
TREK1	AGGGATTTCTACTTGGCGGC	CAAGCACTGTGGGTTTCGTG	99	NM_001017424.3
TRPC1	TGCGTAGATGTGCTTGGGAG	CGTTCCATTAGTTTCTGACAACCG	107	X89066.1

881

882 **Table 2: Sequences, product size, and reference numbers for PCR Primers used in this study.**

883

884

885